



Optimising the use of marine tephrochronology in the North Atlantic: a detailed investigation of the Faroe Marine Ash Zones II, III and IV



Adam J. Griggs^{a,*}, Siwan M. Davies^a, Peter M. Abbott^a, Tine L. Rasmussen^b,
Adrian P. Palmer^c

^a Department of Geography, College of Science, Swansea University, Singleton Park, Swansea SA2 8PP, UK

^b Centre for Arctic Gas Hydrate, Environment and Climate (CAGE), Department of Geology, University of Tromsø, NO9037 Tromsø, Norway

^c Department of Geography, Royal Holloway, Egham Hill, Egham TW20 0EX, UK

ARTICLE INFO

Article history:

Received 10 November 2013

Received in revised form

23 April 2014

Accepted 28 April 2014

Available online 10 June 2014

Keywords:

North Atlantic

Tephra

Taphonomy

Synchronisation

Micromorphology

ABSTRACT

Tephrochronology is central to the INTIMATE¹ goals for testing the degree of climatic synchronicity during abrupt climatic events that punctuated the last glacial period. Since their identification in North Atlantic marine sequences, the Faroe Marine Ash Zone II (FMAZ II), FMAZ III and FMAZ IV have received considerable attention due to their potential for high-precision synchronisation with the Greenland ice-cores. In order to optimise the use of these horizons as isochronous markers, a detailed re-investigation of their geochemical composition, sedimentology and the processes that deposited each ash zone is presented. Shard concentration profiles, geochemical homogeneity and micro-sedimentological structures are investigated for each ash zone preserved within core JM11-19PC, retrieved from the south-eastern Norwegian Sea on the central North Faroe Slope. This approach allows a thorough assessment of primary ash-fall preservation and secondary depositional features and demonstrates its value for assessing depositional integrity in the marine environment. Results indicate that the FMAZ II and IV are well-resolved primary deposits that can be used as isochrons for high-precision correlation studies. We outline key recommendations for future marine tephra studies and provide a protocol for optimising the application of tephrochronology to meet the INTIMATE synchronisation goals.

© 2014 The Authors. Published by Elsevier Ltd. This is an open access article under the CC BY license (<http://creativecommons.org/licenses/by/3.0/>).

1. Introduction

1.1. Synchronisation of disparate climatic archives

Tephrochronology is regarded as one of the key techniques for providing time-synchronous marker horizons which can be used to establish independent and precise tie-points between disparate palaeoarchives (e.g. Hafliðason et al., 2000; Lowe et al., 2008; Davies et al., 2010; Abbott and Davies, 2012). Establishing precise correlation between proxy records is crucial for assessing the degree of climatic synchronicity between different components of the climate system during abrupt climatic shifts of the last glacial period (Austin and Hibbert, 2012; Davies et al., 2012). The geographical range over which tephra can be traced has been extended following the identification of cryptotephra deposits in

ultra-distal locations and as such has increased the number of tie-lines between widely separated archives (e.g. Blockley et al., 2007; Lane et al., 2011; Pyne-O'Donnell et al., 2012). A number of horizons currently exist which enable direct synchronisation between the oceanic and cryospheric realms in the North Atlantic region during the last glacial period (Austin et al., 2004; Davies et al., 2008). However, in order to fully exploit these tie-lines, it is essential to assess the depositional integrity of the tephra horizons in the marine environment – an issue which is currently confounded by the complexity of processes that control deposition in the oceans (e.g. Austin et al., 2004; Brendryen et al., 2010; Abbott et al., 2011). Here we present a detailed geochemical and sedimentological analysis of Marine Isotope Stage (MIS) 2 and 3 (26–50 ka BP) age tephra deposits found in a single North Atlantic marine core (JM11-19PC). We explore the potential depositional processes in order to refine and assess the stratigraphic position of each tephra isochron. This core was selected because of the excellent tephra preservation with ample core material available for the preparation of thin sections.

* Corresponding author. Tel.: +44 1792 295233.

E-mail addresses: 607416@swansea.ac.uk, lake_tahoe4@hotmail.com (A.J. Griggs).

¹ INTIMATE: INTEgrating Ice core, MARine and TERrestrial records 60,000–8000 yrs b2k (EU COST Action ES0907 <http://cost-es0907.geoenvi.org/>).

1.2. Understanding depositional processes in the marine environment: primary vs secondary mixing and taphonomical considerations

The regional dispersal and localised deposition of tephra in North Atlantic marine sequences is the product of several processes occurring aerielly and internally within the ocean system, which in turn influences their applicability as isochronous horizons (Brendryen et al., 2010). One of the fundamental prerequisites of tephrochronology is that tephra is deposited and preserved in a sequence rapidly, i.e. geologically instantaneously, following an eruption (Lowe, 2011). However, tephra shards in the marine realm are subject to both secondary transport and depositional processes (Fig. 1), which potentially introduces stratigraphic and, therefore, chronological uncertainties. These are particularly relevant for cryptotephra deposits that are comprised of a low concentration of glass particles and are thus invisible to the naked eye. Direct sedimentological analysis of tephra and cryptotephra deposits, allied to rigorous geochemical fingerprinting and down-core shard concentration profiles can provide important evidence for the mode of tephra delivery to the seabed. The main modes of tephra delivery from the eruption to the ocean water surface and then through the water column are presented below.

1.2.1. Primary airfall

Following an eruption, tephra is ejected into the atmosphere and primary ash fall deposits are expected to contain a well-sorted distribution, determined by size and density-related processes during the transport of ash through the atmosphere (Sparks, 1981). Thus, a primary airfall deposit will most likely contain a greater concentration of fine-grained tephra particles as the distance from source increases. Primary airfall deposits are also characterised by a homogeneous geochemical population, representing a single eruption, or potentially a couple of homogeneous populations, from very closely-timed eruptions (Brendryen et al., 2010).

1.2.2. Iceberg rafting

Following an eruptive event, an important transport pathway is the proximal deposition of tephra onto ice-sheets which then subsequently undergo calving and rafting to distal locations (Fig. 1) (Brendryen et al., 2010). This process can deliver larger material to a distal depositional site than would typically be associated with primary atmospheric fallout. Iceberg rafting is also dependant on the time taken for the iceberg to calve from the ice-sheet into the ocean; hence it is likely to contain an amalgamation of material sourced from a number of eruptions and different volcanic centres (Ruddiman and Glover, 1972; Lackschewitz and Wallrabe-Adams, 1997; Brendryen et al., 2010). Thus, it is expected that tephra delivered via iceberg rafting would be characterised by a poorly-sorted size distribution and a heterogeneous geochemical signature (Brendryen et al., 2010; Abbott et al., 2011). The identification of co-varying IRD in the succession is a further criterion for identifying iceberg rafting events (Lackschewitz and Wallrabe-Adams, 1997; Davies et al. 2014). Iceberg rafting is likely to compromise the integrity of a tephra horizon by causing a significant temporal delay between the eruption and subsequent deposition into a sedimentary sequence, possibly by up to several millennia (Brendryen et al., 2010). However, it has been suggested that the study of iceberg rafted tephra deposits could aid in the reconstruction of glacial ocean surface circulation patterns (Kuhs et al., 2014).

1.2.3. Sea-ice rafting

Another potentially important transport mechanism is the deposition of tephra onto sea-ice, which can cause time lags of

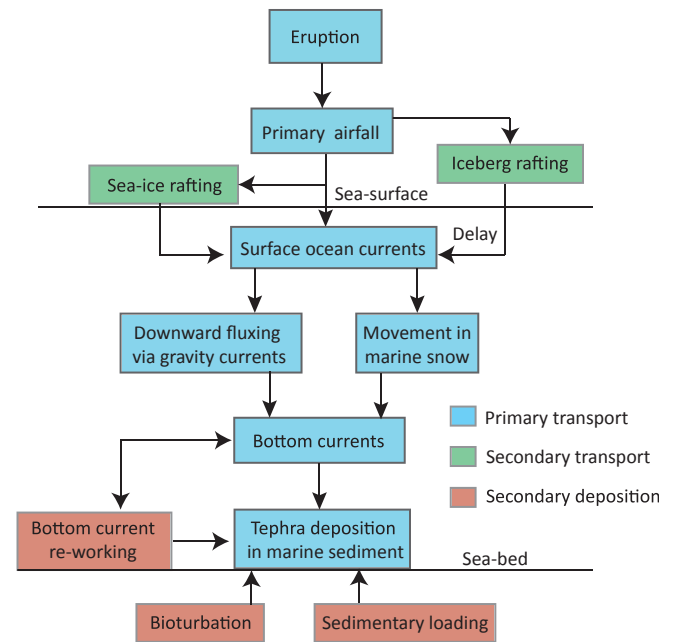


Fig. 1. Schematic summary of the main processes that can influence the transport and deposition of tephra in the marine environment.

years to decades (Brendryen et al., 2010). Although sea-ice persisted permanently in some areas of the North Atlantic during the last glacial, modelling estimates suggest that this was limited to the central Arctic Ocean and areas under the influence of the East Greenland Current, and that sea-ice production was typically seasonal, particularly in the Nordic Seas (Stärz et al., 2012). This prevents the accumulation of multiple eruptions and thus sea-ice rafted deposits are likely to have a homogenous geochemical signature (e.g. Austin et al., 2004). For example, Austin et al. (2004) interpreted that the homogeneous geochemistry and coarser shard sizes of the North Atlantic Ash Zone II (NAAZ II) in MD95-2006, was indicative of initial airfall deposition and subsequent transport to the core site by sea-ice. However, coarser shard sizes are not always a diagnostic indicator of sea-ice rafting, as fine-grained glass shards can also be transported long distances on sea-ice. Whilst this mechanism can increase the regional dispersal of tephra, it is unlikely to affect a deposits integrity as an isochron because the temporal lag is far less than the sampling resolution of marine sequences. As this mechanism does not involve calving from ice sheets, the deposit is unlikely to be associated with a coeval IRD signal.

1.2.4. Ocean currents

Following tephra deposition onto the ocean surface by means of wind, iceberg rafting or sea-ice rafting, the glass shards will move from the surface down to the seabed (Wallrabe-Adams and Lackschewitz, 2003). Laboratory experiments demonstrate that vertical density currents generated by ash loading allow the movement of particles to overcome strong density gradients in the ocean and transport ash one to three orders of magnitude faster than is possible by Stokes settling Law (Manville and Wilson, 2004). Wallrabe-Adams and Lackschewitz (2003) hypothesised that glass particles could be transported laterally over a relatively large distance (20–55 km) during the sinking process. However, rapid settling of ash particles implies that the transport through the water column would not affect the chronological integrity of the deposit. Although residence time in

the water column can be affected by turbulence and salinity boundaries (Manville and Wilson, 2004), this is unlikely to keep a shard in suspension for more than a few days to weeks, since tephra is likely to fall through the water column within marine snow (Fig. 1). For example, Wiesner et al. (1995) demonstrated that the vertical oceanic settling velocities into deep-water sediment traps in the South China Sea were >2 cm/s following the paroxysmal phase of the Pinatubo eruption in 1991.

One process that may disturb this signal, however, is redistribution and erosion by bottom currents. Michels (2000) calculated that geostrophic bottom current velocities may range from 25 to 36 cm/s in the Nordic Seas during storm events, which may influence the spatial distribution of tephra, resulting in distinct variations in horizon thickness and glass shard concentration in nearby cores (Wallrabe-Adams and Lackschewitz, 2003). Thus, an increase in bottom currents during interstadials and storm events may remobilise material from previously deposited eruptions. Any bottom-current induced erosion is likely to mobilise tephra material and produce an upward gradational distribution or tail-off in shard concentration (e.g. Abbott et al., 2013, 2014). Thus, for cryptotephra deposits, an upward tail in concentration from a main peak would be expected to have a corresponding homogeneous geochemical signature throughout the deposit. However, material from older eruptions may become remobilised and transported from one site to another, resulting in the deposition of material sourced from a number of different events. This reinforces the need for careful scrutinisation of cryptotephra shard concentration profiles together with an assessment of geochemical results from several intervals within these deposits (Abbott et al. 2014; Davies et al., 2014).

1.2.5. Post-depositional reworking of material

Following deposition of tephra onto the seabed, as well as being reworked by bottom currents, tephra is also susceptible to bioturbation (Abbott et al., 2011). Characteristic sedimentological evidence of bioturbation includes a gradational upper contact that is spread over several centimetres which introduces a number of stratigraphical uncertainties (Manville and Wilson, 2004; Lowe, 2011). Low concentrations of shards below the peak are also considered to be a signature of bioturbation, although this is unlikely to affect the position of the peak in shard concentration (Ruddiman and Glover, 1972). Remobilisation of material can also occur as a result of turbidity currents, and present-day tephrostratigraphic techniques are not sufficient to isolate the complex interplay of post-depositional processes and pinpoint the modification mechanisms at work.

However, recent investigations by Matthews et al. (2011) examined the potential of micromorphology to identify micro-sedimentological structures within tephra deposits from a marine core in the Southern Adriatic. This work identified features associated with turbidite deposition, bioturbation and additional micro-scale evidence of gravitational loading and re-sedimentation. Micro-morphological analysis of sediment structures has the potential to provide additional supporting evidence for understanding the taphonomic processes associated with tephra deposition. When combined with the detailed analysis of the tephra geochemistry, shard distribution and particle size analysis, this approach provides a more precise assignment of tephra and in the marine environment. We adopt this approach to investigate three ash zones in one marine core and assess its potential value for the examination of tephra and cryptotephra deposits in this sedimentary environment.

1.3. The Faroe Marine Ash Zones: optimising their employment as time-stratigraphic marker horizons

Tephra deposits in North Atlantic marine sediments, mainly retrieved from the IRD belt, were originally described by Bramlette and Bradley (1941) and later by Ruddiman and Glover (1972), who named these horizons the 'North Atlantic Ash Zones' (NAAZ I and II). Investigations in the Faroes region during the past decade have identified 4 new tephra deposits, 'Faroe Marine Ash Zones' (FMAZ) I, II, III and IV (Rasmussen et al., 2003; Wastegård et al., 2006; Wastegård and Rasmussen, 2014), although only the latter three horizons, fall within the time-interval of this investigation.

FMAZ II was first discovered in marine cores near the Faroe Islands as a black visible horizon that varied from 2 to 10 cm in thickness and was thought to have been deposited via primary airfall (Rasmussen et al., 2003). This tephra has since been discovered in the Labrador Sea, NE Atlantic, and the Greenland ice cores ($26,740 \pm 390$ a $b2k^2$) (Wastegård et al., 2006; Davies et al., 2008; Svensson et al., 2008; Austin et al., 2012). According to the NGRIP stratigraphic position, the tephra falls within a cold period ca. 1000 years after the onset of Greenland Interstadial (GI) -3 which is consistent with its position in the marine cores, suggesting a close coupling of the atmospheric and oceanic systems during this time (Davies et al., 2008).

FMAZ III was originally described in the Faroes region as the '33 ka tephra', where it forms a visible scattered tephra zone spanning the transition into the peak warmth of Dansgaard-Oeschger (DO) event 8, identified in the ratio between planktonic to benthic foraminifera abundances (Rasmussen et al., 2003; Wastegård et al., 2006). Davies et al. (2010) proposed the correlation of a NGRIP tephra at 2066.95 m ($38,122 \pm 723$ a $b2k^2$) to the FMAZ III, which suggested deposition ca 100 years after the onset of the GI-8 warming. However, Bourne et al. (2013) have subsequently discovered a suite of tephra layers in the NGRIP and NEEM ice-cores that represent 14 volcanic events between Greenland Stadial (GS) 9 and GI-8 – all of which fall within the compositional range of the FMAZ III found within the Faroes region. As such, Bourne et al. (2013) suggest that the FMAZ III most likely represents a complex ash zone in the marine environment made up of material from several closely-timed eruptions. This has major implications for establishing tephra correlations between ice core and marine records at this time and a re-evaluation of this deposit is required to assess whether individual stratigraphic horizons seen in the ice can be resolved in the marine realm.

The FMAZ IV is a recent discovery and appears as a thick black horizon in a number of marine cores in the Faroe Shetland Channel (Wastegård and Rasmussen, 2014). The horizon is thought to have been deposited during DO-12 and dates to ca. 47,000 years BP according to age model estimates (Wastegård and Rasmussen, 2014).

Initial work on the FMAZs focused on shards >150 μ m in diameter (Rasmussen et al., 2003; Wastegård et al., 2006). Our study builds upon these investigations and employs cryptotephra extraction techniques to additionally explore the fine-grained fraction (25–150 μ m) and present a contiguous shard concentration profile within a single marine core from the Faroes region. These profiles are considered alongside detailed geochemical results obtained from three separate grain-size fractions to capture the full compositional range of these tephra deposits. Micro-sedimentological structures across the depositional contacts are also investigated to refine the stratigraphical placement of the tephra isochron.

² Age uncertainties are reported as 1-sigma corresponding errors for the GICC05 chronology following Svensson et al. (2008).

2. Methodology

2.1. Core recovery and measurements

The JM11-19PC core was retrieved onboard the R-V Jan Mayen in May 2011 from 1179 m water depth on the central North Faroe Slope in the Southeastern Norwegian Sea ($62^{\circ}48'98''$ N $03^{\circ}52'04''$ E) (Fig. 2). The core is ~11 m long and penetrates into MIS 6 sediments at the base. In this investigation we examine the depth interval between 183 and 558 cm, covering MIS 2 and part of MIS 3. Whole core magnetic susceptibility was measured onboard using a Geotek MSCL core loop sensor following procedures outlined in Rasmussen et al. (1996).

2.2. Density separation and identification of tephra shards

The tephra content of the core sequence between 183 and 558 cm depth was initially investigated at a 5 cm contiguous resolution and then intervals of elevated shard concentrations were further analysed at a 1 cm resolution. The samples were prepared and quantified according to the methodology outlined in Turney (1998) and Blockley et al. (2005) and modified for marine tephra by Abbott et al. (2011, 2013). Sediment samples were freeze dried and 0.5 g of dry weight sediment for each sample was weighed for tephra analysis. The sediment was then immersed in dilute HCl (10%) overnight to remove carbonate material. Each sample was subsequently wet-sieved into three separate grain-size fractions ($>125\ \mu\text{m}$, $80\text{--}125\ \mu\text{m}$ and $25\text{--}80\ \mu\text{m}$). The $25\text{--}80\ \mu\text{m}$ fraction was density separated into three fractions using the heavy liquid sodium polytungstate to aid the isolation of rhyolitic ($2.3\text{--}2.5\ \text{g/cm}^3$) and basaltic grains ($>2.5\ \text{g/cm}^3$). Material from the $>125\ \mu\text{m}$, $80\text{--}125\ \mu\text{m}$ and $25\text{--}80\ \mu\text{m}$ ($2.3\text{--}2.5\ \text{g/cm}^3$) fractions was mounted in Canada Balsam on microscope slides and inspected for tephra content using optical microscopy. Material with a density of $>2.5\ \text{g cm}^3$ was magnetically separated to purify the basaltic material.

2.3. Magnetic separation and spiking of basaltic tephra shards

Basaltic tephra exhibits ferromagnetic properties, mainly due to the high Fe content and through the influence of paramagnetic elements such as Al, Mg and Na (Walden et al., 1999). This allows tephra shards to be separated when a magnetic current is applied. Such separation significantly reduces the amount of non-magnetic particles, particularly quartz, in the sample of interest, improving efficiency during optical identification of basaltic tephra (Froggatt and Gosson, 1982). Previous use of magnetic separation to aid the isolation of basaltic material from other mineral components has demonstrated the efficiency that this technique can achieve by alteration of the magnetic field strength and the forward/sideway tilt of the apparatus (Froggatt and Gosson, 1982; Mackie et al., 2002).

With the use of a Frantz IsoDynamic Magnetic Separator, a series of experiments were conducted on ten different marine samples from a nearby Faroe Islands core (LINK 16) with previously quantified shard counts (Abbott et al., 2014). The magnetic current, tilt and slope were altered at intervals of 0.05 nA between 0.60 and 1.00 nA and five degrees between -15° and 25° respectively and the total number of separated basaltic shards in the magnetic fraction was determined. Two replicates of each sample were processed. The parameters that delivered the most effective recovery of tephra were identified as a current of 0.85 nA, tilt of -15° and a slope of 22.5° (Fig. 3). These parameters were then used to quantify the number of basaltic glass shards present within the JM11-19PC sequence.

A palynological quantification technique, previously applied to the study of tephra by Gehrels et al. (2006) and Bourne (2012) was employed due to the exceptionally high number of basaltic glass shards in the $>2.5\ \text{g/cm}^3$ fraction. A Lycopodium spore tablet was added to the magnetically-separated residue and dissolved in 5 ml of distilled water in a centrifuge tube. These samples were placed in a water bath at $50\ ^{\circ}\text{C}$ for two hours to ensure complete dissolution of the tablet. A dilute (10%) solution of HCl (2 ml) was then added to the

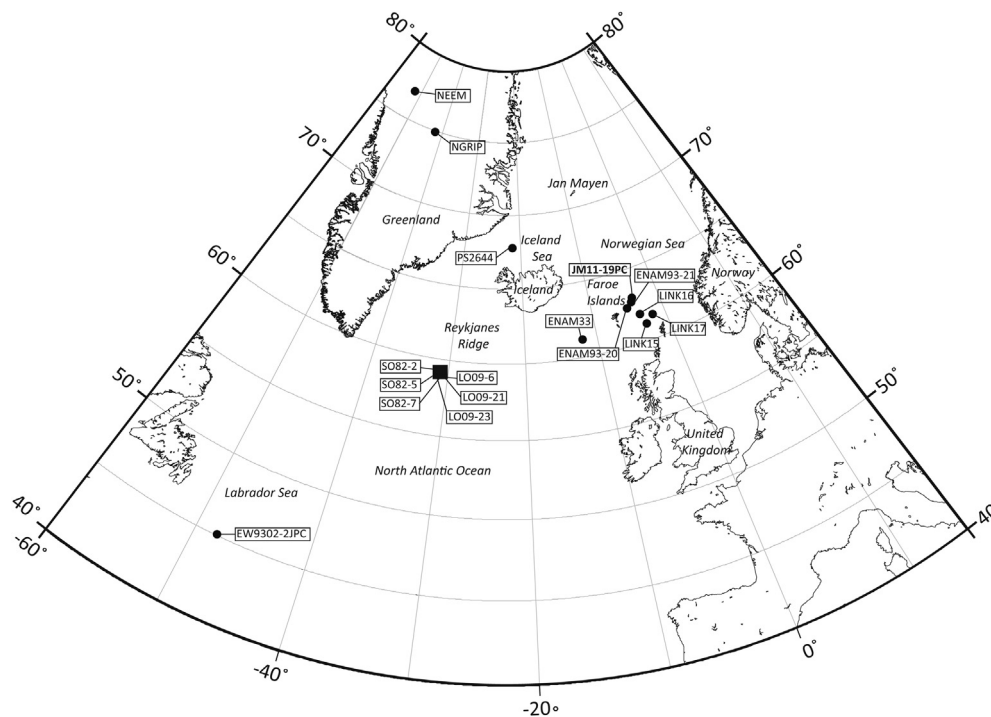


Fig. 2. Location map of the coring sites for JM11-19PC and Greenland ice and North Atlantic marine cores referred to in the text.

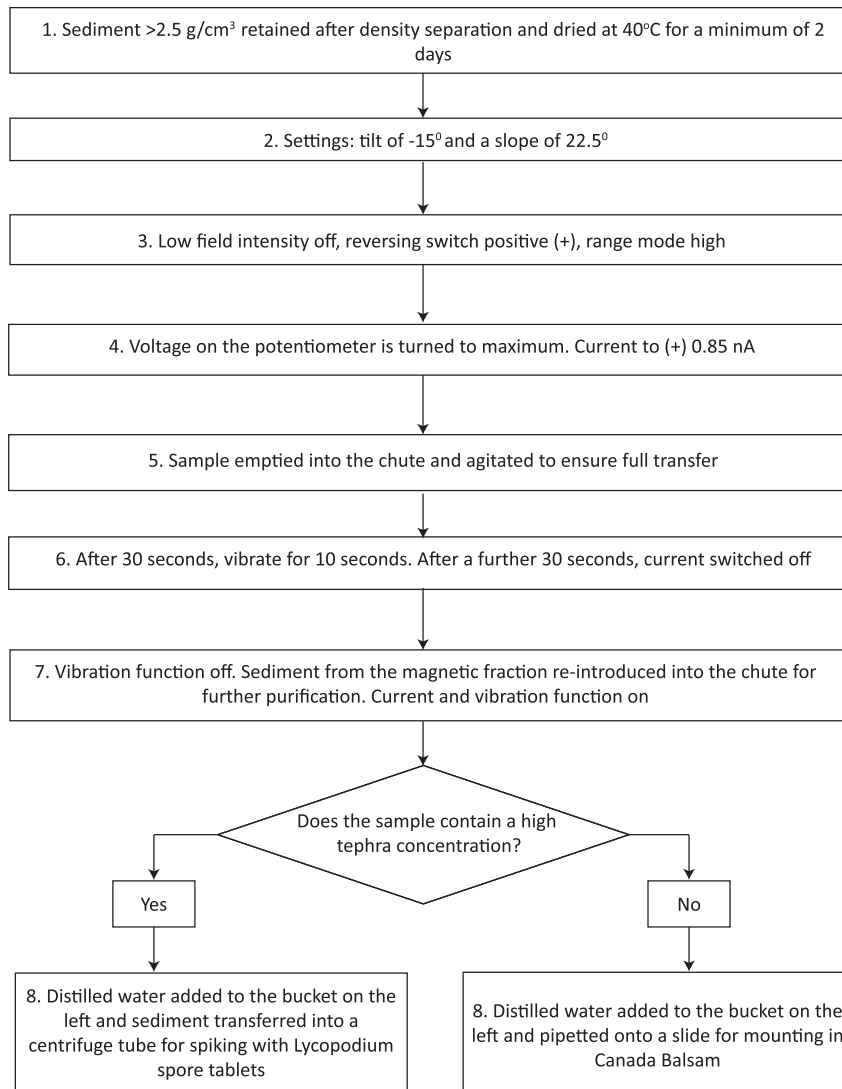


Fig. 3. Summary of protocol for the magnetic separation of basaltic shards from mineral-rich sediments.

solution to remove any remaining sodium bicarbonate. The spiked sample was washed three times with distilled water by centrifugation and finally 5 ml of distilled water was added to the centrifuge tube. The solution was shaken vigorously to mix the sample and eight drops of the mixture were pipetted onto a microscope slide and mounted in Canada Balsam. This amount was deemed to be the optimum volume to cover the slide beneath the cover slip, similar to the 500 μ l recommended by Gehrels et al. (2006). Glass shards were counted alongside Lycopodium spores in each sample across three vertically-defined transects per slide. The concentration of tephra shards, C , was calculated using (Eq. (1)):

$$C = l \times \left(\frac{a}{bd} \right) \quad (1)$$

Where a) is the glass shard count, b) is the Lycopodium spore count, d) is the sample dry weight and l) is the number of Lycopodium spores in each tablet ($n = 20,848$) according to the manufacturer estimate determined using an electronic particle counter. This methodology was adapted for the high-resolution sampling intervals, where three tablets (i.e. 62,544 spores) were added to the magnetically-separated residue due to the exceptionally high glass shard concentrations.

2.4. Geochemical characterisation of glass shards

Glass shards were extracted for major element geochemical analysis from each grain-size fraction. Samples were processed according to the methodology outlined above and then mounted in epoxy resin on glass slides. The slides were then ground using silicon carbide paper and polished using 9, 6 and 1 μ m diamond suspension to expose polished glass shard surfaces for electron-probe microanalysis (EPMA). The oxide concentrations of ten major and minor elements were analysed using wavelength-dispersive EPMA at the Tephrochronological Analytical Unit at the University of Edinburgh, using a Cameca SX100 electron microprobe equipped with five vertical WD spectrometers. The operating conditions are modified from Hayward (2012) and are outlined in the Supplementary information. Pure metals, simple silicate minerals and synthetic oxides, including andradite were used for calibration, and the secondary standards Lipari and BCR2g were analysed regularly to monitor elemental drift and to assess the accuracy of the shard analyses. Glass shards preserved in the marine realm are susceptible to variable levels of post-depositional hydration (Wallrabe-Adams and Lackschewitz, 2003; Abbott et al., 2011). As such the results of the EPMA analysis were normalised to 100% total oxide values (i.e. an anhydrous basis) to

remove any variability that may be apparent when comparing datasets from different depositional environments that have not experienced comparable levels of post-depositional hydration (Abbott et al., 2011; Pearce et al., 2014). All analyses with total oxide values <94% were rejected. All raw data values are provided in the Supplementary information (see Tables 1–3). Similarity coefficient (SC) comparisons were employed using the methods outlined in Borchardt et al. (1972) and Begét et al. (1992).

2.5. Thin-section preparation

Undisturbed sediment samples were extracted in U-channels (20 × 20 mm) spanning the onset of tephra deposition and the decline in tephra shard deposition associated with each of the three ash zones. Thin-sections were prepared following the procedures outlined in Palmer et al. (2008), including the application of acetone replacement methods to limit cracking of silty clay sediment during drying (van der Meer and Menzies, 2011). Each thin-section was polished to a thickness of between 25 and 35 μm .

3. Results

3.1. Tephrostratigraphy, geochemistry and micromorphology

The tephrostratigraphy for JM11-19PC is presented in Fig. 4. Three distinct tephra deposits, composed of brown shards, were observed in the $>2.5 \text{ g/cm}^3$ (25–80 μm), 80–125 μm and $>125 \mu\text{m}$ fractions, spanning the position of the visible tephra horizons. Each deposit exhibits distinct peaks in shard concentration relative to background values. Geochemical results reveal that each major

peak is made up of material with a basaltic composition (Fig. 5, Table 1).

3.2. FMAZ II

3.2.1. Tephrostratigraphy: JM11-19PC 298–308 cm

A visible black macrotephra forms a distinct 1 cm-thick horizon between 304 and 305 cm depth and coincides with the highest shard concentration (>4 million shards gdw in the 25–80 μm fraction and 147 in the $>125 \mu\text{m}$ fraction). A sharp increase and decrease in shard concentration profile over 6 cm suggests a rapid pulse of tephra with limited post-depositional re-working. The shards have a dark brown colour, dense blocky morphology and some are slightly vesicular in appearance.

3.2.2. Micro-sedimentology

There are two distinct units in this section. The first occurs between 307 and 304.5 cm and consists of a poorly-sorted silty clay with occasional tephra shards ($\sim 55 \mu\text{m}$ in diameter; $n = 20$), distributed within the matrix (Fig. 6a). Toward the top of this unit, there are occasional ($\sim 1\text{--}3 \text{ mm}$) lenses of well-sorted tephra grains up to $\sim 200 \mu\text{m}$ in size within the host sediment. These lenses are irregular, aligned horizontally or vertically within the host sediment (Fig. 6b) and generally composed of sediment from Unit 2. The second unit identified between 304.5 cm and 298 cm is composed of well-sorted, abundant tephra shards dominated by the size fraction of 25–80 μm (Fig. 6d). The unit has a sub-horizontal, sharp contact at 304–304.5 cm depth (Fig. 6c). There is evidence of discrete lobate structures below this level. Here, below the contact, material from unit 2 has penetrated into unit 1.

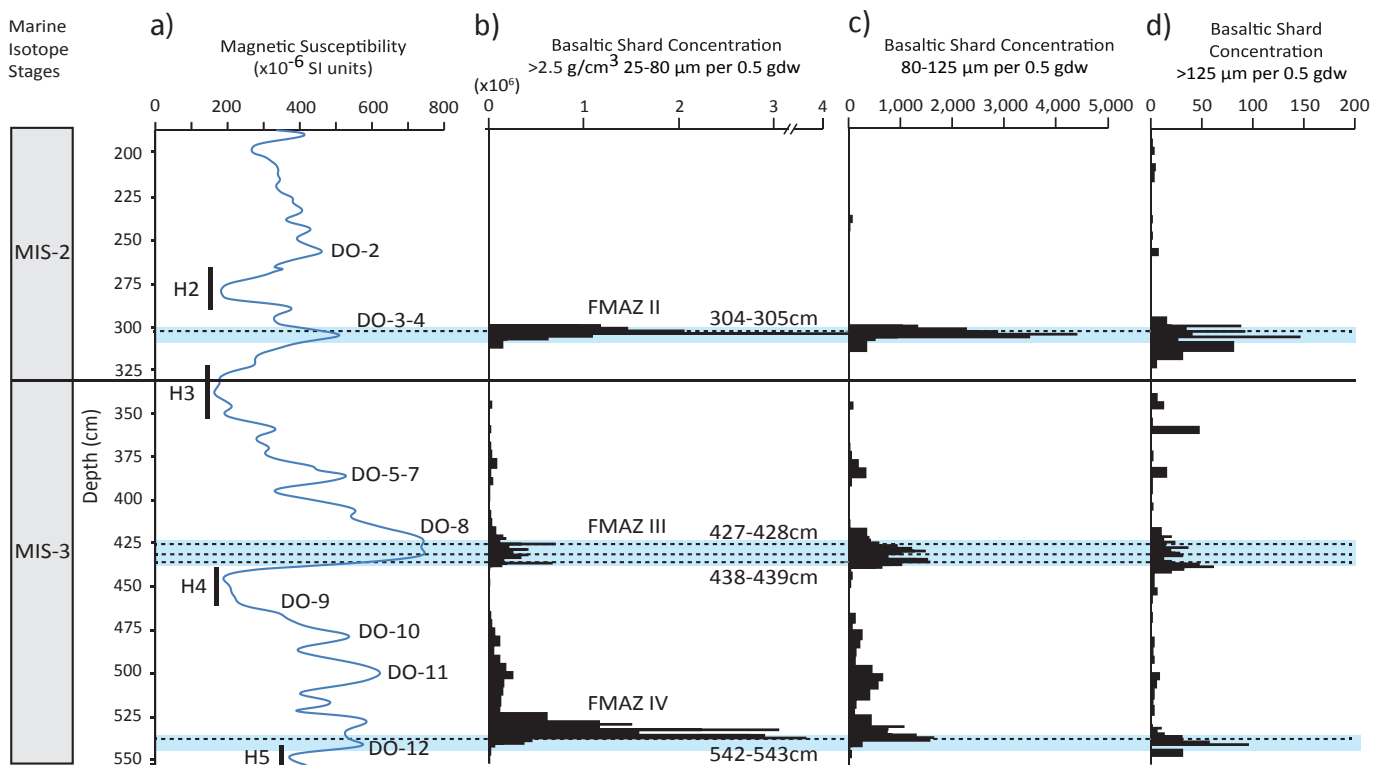


Fig. 4. Tephra stratigraphy for MIS 2 and late MIS 3 section from the JM11-19PC core. a) Magnetic susceptibility b) Number of basaltic shards with a density $>2.5 \text{ g/cm}^3$ within the 25–80 μm fraction. c) Number of basaltic shards within the 80–125 μm fraction. d) Number of basaltic shards within the $>125 \mu\text{m}$ fraction. Grey dotted lines denote samples for which glass shards were extracted for geochemical analysis. The shaded blue area denotes the depth intervals sampled for thin section analysis (see Fig. 6). H = Heinrich event approximate positions. DO = Dansgaard-Oeschger event and the number denotes the associated Greenland Interstadial event following the recommendations of Rasmussen et al. (2014). gdw = grams dry weight sediment. (For interpretation of the references to colour in this figure legend, the reader is referred to the web version of this article.)

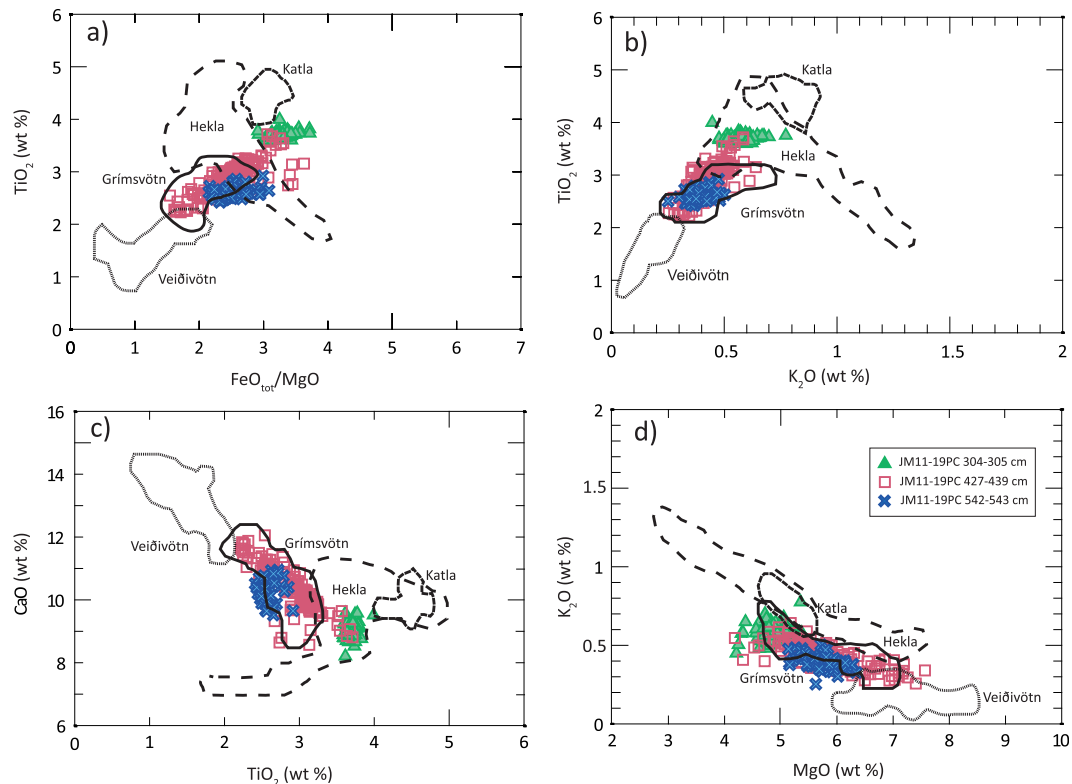


Fig. 5. Glass shard analyses for the 3 FMAZs in JM11-19PC compared to geochemical envelopes for different source volcanoes based on individual whole rock analyses presented in Jakobsson (1979), Boyle (1994), Larsen et al. (2002), Óladóttir et al. (2008) and Jakobsson et al. (2008). Data have all been normalised to 100% total oxide concentrations.

These features are most easily explained as loading structures. The tephra becomes less densely concentrated in the upper part of this unit and more mixed within the coarse-silty clay matrix (Fig. 6d). The visible tephra component has a similar shard size throughout this unit and no grading is observed.

3.2.3. Geochemistry and wider correlations; JM11-19PC 304–305 cm

In total, 85 shards form a distinct homogeneous population (Fig. 7), with only four clear outliers in the coarser $>125\ \mu\text{m}$ fraction and one in the $25\text{--}80\ \mu\text{m}$ fraction. Distinctive geochemical characteristics include SiO_2 concentrations of $\sim 47.7\text{--}51.0\ \text{wt}\%$, TiO_2 concentrations of $\sim 3.7\ \text{wt}\%$, CaO concentrations of $\sim 8.2\text{--}9.6\ \text{wt}\%$, K_2O concentrations between ~ 0.4 and $0.8\ \text{wt}\%$ and $\text{FeO}_{\text{tot}}/\text{MgO}$ ratios between ~ 2.8 and 3.7 (see Table 1). These characteristics are typical of a transitional alkali basaltic composition, suggesting a source from the Eastern or Southern Icelandic flank zones (Jakobsson, 1979). Comparisons with proximal Icelandic material demonstrate that the distinct geochemical population has a close affinity to material sourced from the Hekla/Vatnafjöll system (Fig. 5) (Jakobsson, 1979; Larsen, 1981; Lackschewitz and Wallrabe-Adams, 1997; Davies et al., 2008; Jakobsson et al., 2008).

Glass shard analyses from JM11-19PC show strong affinity with FMAZ II preserved in five other marine cores from the Faroes region and the NGRIP ice-core with an average similarity coefficient of 0.98 (Rasmussen et al., 2003; Wastegård et al., 2006; Davies et al., 2008). JM11-19PC and the NGRIP data-set exhibit a tighter geochemical population than observed for the other marine cores (Fig. 7). The wider geochemical scatter of shards from previously published Faroes cores and EW 9302-JPC in the Labrador Sea potentially extends the full compositional range of this eruption. Alternatively, this scatter may be the result of bottom current reworking (see Discussion 4.1.1 below). We also note that no shards

investigated in this study fall within the FMAZ II-2 sub-population originally identified by Wastegård et al. (2006) (Fig. 7).

The geochemical population of JM11-19PC 304–305 cm also displays some affinities to the V1 ash zone deposited in marine cores on the Reykjanes Ridge (Lackschewitz and Wallrabe-Adams, 1997). According to the magnetic susceptibility record from JM11-19PC and a few radiocarbon dates and IRD record from the Reykjanes Ridge, the V1 ash zone falls in a similar stratigraphic position to the 304–305 cm horizon (Lackschewitz and Wallrabe-Adams, 1997). The V1 deposit, however, is heterogeneous (Fig. 7) and co-varies with high IRD, a diagnostic feature of iceberg rafted deposits. However, a notable sub-peak, SO82-5-V1x-KAL, contains a homogenous population with no coeval IRD signal and exhibits a high similarity coefficient value of 0.95 with JM11-19PC 304–305 cm (Fig. 7).

3.3. FMAZ III

3.3.1. Tephrostratigraphy: JM11-19PC 423–443 cm

This deposit straddles the warming transition of DO-8 (Fig. 4). The deposit forms a complex and diffuse zone of tephra which exhibits 2 minor peaks in shard concentration in the $25\text{--}80\ \mu\text{m}$ fraction, although the tephra is not visible to the naked eye. These peaks in the fine-grained fraction are not mirrored in the coarser-grained fractions, which contain multiple peaks across 13 cm and are offset from the $25\text{--}80\ \mu\text{m}$ peaks in concentrations (Fig. 4). Total shard concentrations per 0.5 gdw do not exceed $\sim 700,000$ in the fine fraction and 62 shards in the coarse ($>125\ \mu\text{m}$) fraction, which is significantly less than the other deposits examined within this study. Glass shards from each of the peaks at 438–439 cm and 427–428 cm in all grain-size fractions and the mid-point at 434 cm ($25\text{--}80\ \mu\text{m}$ fraction only) were extracted and prepared for geochemical analysis. In total, 173 glass shards were analysed for geochemistry. A correlation of the JM11-19PC tephra record with

Table 1

Mean and 1σ major element results of glass shards extracted from the main populations for the FMAZ II, III and IV. Total oxide values are raw values prior to normalisation. All major elements are expressed as percentage weight. Total iron is expressed as FeO. n = number of shards analysed. Two different EPMA operating setups were used. For the first setup, three sets of column conditions were employed. Firstly, Na₂O and Al₂O₃ were determined using an accelerating voltage of 15 kV and a beam current of 0.5 nA. Secondly, MgO, K₂O, CaO, FeO and SiO₂ were determined using an accelerating voltage of 15 kV and a beam current of 2 nA. Thirdly, P₂O₅, TiO₂ and MnO were determined using accelerating voltage of 15 kV and a beam current of 60 nA. A 4 μ m beam diameter was used throughout. Counting times were 20 s at the peak position and 10 s for background for all elements except MnO (60 and 60 s). For the second EPMA setup two column conditions were used. Na₂O, MgO, Al₂O₃, SiO₂, K₂O, CaO, and FeO were determined using an accelerating voltage of 15 kV and a beam current of 2 nA and P₂O₅, TiO₂, and MnO were determined using an accelerating voltage of 15 kV and a beam current of 60 nA. A 5 μ m beam diameter was used throughout. Counting times were 20 s at the peak position and 10 s for background for all elements except TiO₂ (30 and 15 s), MnO (50 and 40 s) and FeO (40 and 20 s). The full data-set and reference values are given in the [Supplementary file](#).

Tephra layer	Depth (cm)	Grain size (μ m)	n	SiO ₂	TiO ₂	Al ₂ O ₃	FeO	MnO	MgO	CaO	Na ₂ O	K ₂ O	P ₂ O ₅	Total
FMAZ II	304–305	25–80	22	50.13	3.71	12.77	15.35	0.24	4.78	8.92	3.05	0.56	0.48	97.68
				0.44	0.09	0.30	0.51	0.01	0.27	0.26	0.33	0.06	0.04	1.18
FMAZ II	304–305	80–125	41	49.49	3.70	13.15	15.33	0.25	4.83	9.15	3.13	0.57	0.41	97.34
				0.64	0.05	0.38	0.50	0.01	0.19	0.20	0.25	0.05	0.02	1.37
FMAZ II	304–305	>125	22	50.14	3.70	12.70	15.34	0.24	4.75	9.10	3.06	0.59	0.39	98.05
				0.30	0.04	0.36	0.34	0.01	0.19	0.21	0.12	0.05	0.02	0.80
FMAZ II Average	304–305	25–80, 80–125, >125	85	49.82	3.70	12.93	15.34	0.24	4.80	9.08	3.09	0.57	0.42	97.61
				0.61	0.06	0.41	0.46	0.01	0.21	0.23	0.25	0.05	0.04	1.22
FMAZ III	427–428	25–80	25	49.94	2.99	13.16	14.18	0.23	5.68	10.38	2.75	0.43	0.26	98.54
				0.43	0.30	0.42	0.97	0.01	0.56	0.70	0.26	0.08	0.04	0.75
FMAZ III	427–428	80–125	28	49.46	2.86	13.40	13.87	0.22	6.01	10.56	2.91	0.42	0.27	97.78
				0.51	0.40	0.64	1.09	0.02	0.72	0.80	0.27	0.10	0.06	1.55
FMAZ III	427–428	>125	8	49.62	2.61	13.66	13.00	0.21	6.43	11.13	2.73	0.37	0.23	98.05
				0.30	0.28	0.28	0.71	0.01	0.54	0.47	0.16	0.06	0.04	0.86
FMAZ III	434–435	25–80	23	49.96	3.02	12.98	14.49	0.23	5.54	10.15	2.89	0.46	0.27	98.36
				0.43	0.28	0.37	0.74	0.02	0.52	0.55	0.19	0.07	0.03	1.07
FMAZ III	438–439	25–80	24	49.97	3.03	13.06	14.24	0.23	5.66	10.18	2.91	0.46	0.26	98.76
				0.37	0.26	0.37	0.71	0.01	0.47	0.51	0.21	0.06	0.03	0.89
FMAZ III	438–439	80–125	25	49.89	2.95	13.12	14.08	0.22	5.83	10.38	2.86	0.42	0.26	98.89
				0.40	0.21	0.28	0.79	0.01	0.49	0.51	0.17	0.06	0.02	0.97
FMAZ III	438–439	>125	23	49.73	2.90	13.26	13.98	0.22	6.00	10.38	2.85	0.42	0.27	98.31
				0.32	0.30	0.47	1.02	0.02	0.53	0.62	0.13	0.05	0.04	0.70
FMAZ III Average	427–439	25–80, 80–125, >125	156	49.81	2.94	13.20	14.07	0.23	5.83	10.38	2.85	0.43	0.26	98.42
				0.44	0.31	0.47	0.93	0.02	0.59	0.65	0.22	0.07	0.04	1.09
FMAZ IV	542–543	25–80	25	50.58	2.56	13.26	14.17	0.23	5.67	10.09	2.80	0.39	0.23	98.18
				0.36	0.09	0.23	0.47	0.01	0.27	0.28	0.12	0.05	0.01	0.78
FMAZ IV	542–543	80–125	32	50.11	2.59	13.30	14.24	0.23	5.76	10.30	2.84	0.40	0.23	97.83
				0.46	0.09	0.24	0.57	0.01	0.33	0.35	0.23	0.04	0.02	1.08
FMAZ IV	542–543	>125	14	50.34	2.63	13.23	13.93	0.23	5.84	10.46	2.71	0.40	0.23	98.24
				0.38	0.12	0.28	0.49	0.01	0.27	0.36	0.18	0.06	0.02	0.86
FMAZ IV Average	542–543	25–80, 80–125, >125	71	50.32	2.59	13.27	14.15	0.23	5.75	10.26	2.80	0.39	0.23	98.03
				0.46	0.10	0.24	0.53	0.01	0.30	0.36	0.19	0.04	0.02	0.95

that of a neighbouring core (ENAM93-21) suggests that no coeval IRD signal is associated with the FMAZ III deposit (Fig. 8).

3.3.2. Micro-sedimentology

This deposit is composed of a single unit from 443 to 423 cm and contains massive, poorly-sorted coarse silty clay (Fig. 6ii). Tephra shards, ~45 μ m in diameter ($n = 20$), are randomly distributed within the host sediment, although there are occasional small (~1 mm) sub-horizontal and irregular lenses of tephra concentrated within the unit (Fig. 6e). There are no distinct micro-sedimentological features that coincide with the peaks in shard concentration (Fig. 6ii).

3.3.3. Geochemistry and wider correlations JM11-19PC 427–439 cm

Distinctive geochemical characteristics of this deposit include SiO₂ contents of ~48.5–51.1 wt%, K₂O concentrations of ~0.4 wt%, TiO₂ concentrations of ~2.3–3.7 wt%, CaO concentrations of ~8.8–12.1 wt% and MgO concentrations between ~4.7 and 7.6 wt% (Fig. 9). These characteristics are typical of a tholeiitic basaltic composition, with the TiO₂ and K₂O concentrations implying an origin from the Grímsvötn system (Jakobsson, 1979) (Fig. 5). Although a volcanic source can be determined for the deposit, glass shards from each individual depth sample occupy

the full range of Grímsvötn-sourced material. Each grain-size fraction from 438 to 439 cm appears to exhibit a relatively tight population, although no other distinct populations can be observed for the other depth-intervals that have been analysed. Moreover, biplots of TiO₂ vs CaO and FeO_{tot}/MgO vs TiO₂ highlight the heterogeneity and wide range of values for these oxides (Fig. 9d).

Seventeen outlier shards are found in this deposit and appear unrelated to the main FMAZ III population and cannot be regarded as additional sub-populations (Fig. 9a). Although six of these shards fall within the FMAZ III-2 envelope, previously defined by Wastegård et al. (2006), we do not believe that this sub-population is present within JM11-19PC due to the low number of analyses that fall within this envelope.

Glass shard analyses from the main geochemical population show strong similarities and a similarity coefficient of 0.98 with FMAZ III deposits from three other marine cores in the Faroes region (Rasmussen et al., 2003; Wastegård et al., 2006) (Fig. 9). The geochemical composition of these previously published deposits exhibit a near-identical spread to the JM11-19PC 427–439 cm deposit. This can be clearly observed on TiO₂ vs CaO and FeO_{tot}/MgO vs K₂O geochemical biplots (Fig. 9a and b).

Wastegård et al. (2006) proposed that a correlation may exist between the V2 ash zone and the FMAZ III. The V2 ash zone has

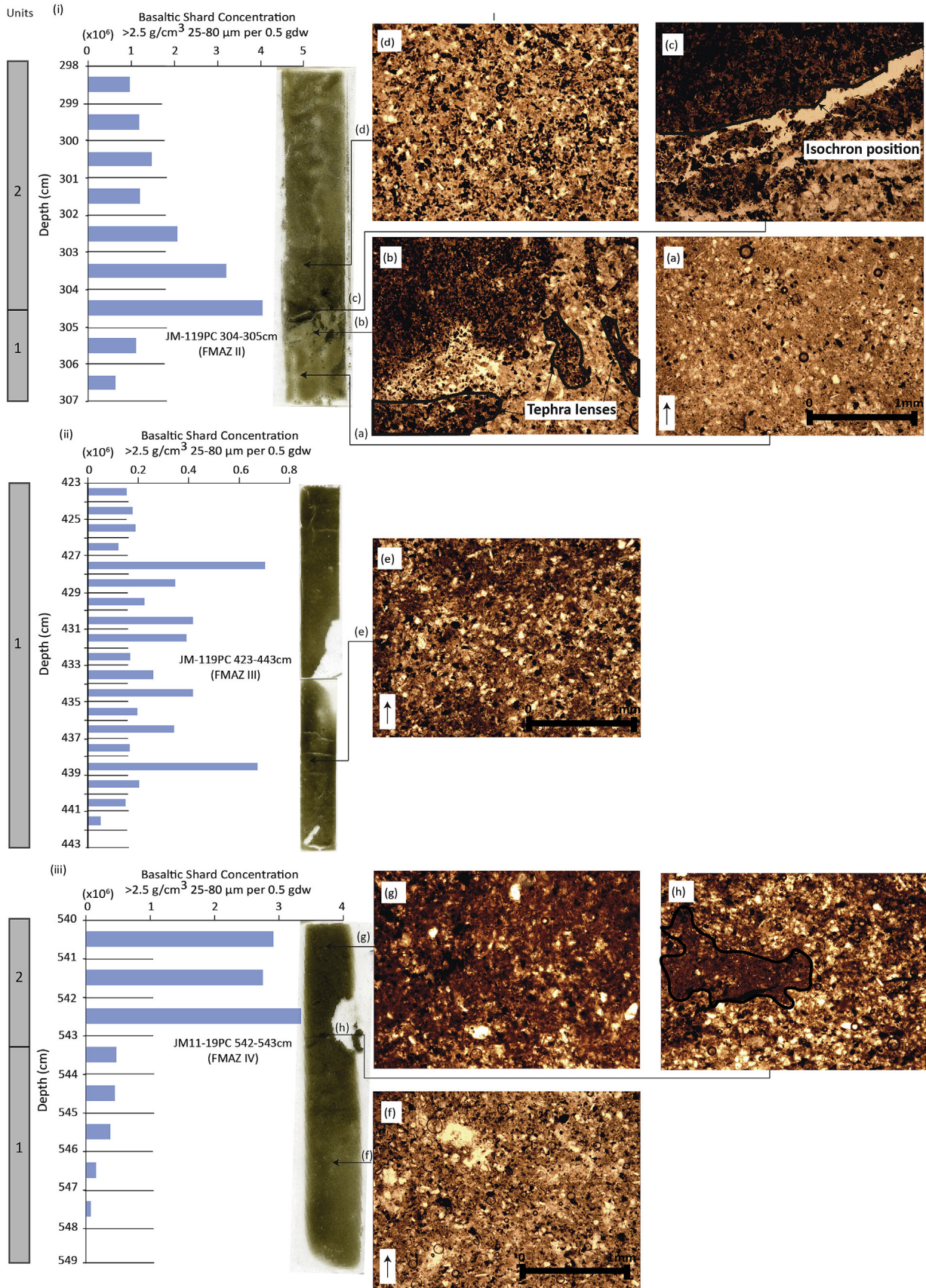


Fig. 6. Thin-section micromorphology images aligned to high-resolution shard concentration profiles (25–80 μm fraction) across each ash zone. Indicative microfacies features observed throughout each of the FMAZ deposits are presented. Units 1 and 2 are defined according to the micro-sedimentological features observed. (i) FMAZ II deposit (a) unit 1 (307–304.5 cm) with a massive, relatively poorly-sorted matrix of silty clay. Light and dark brown glass shards are dispersed in relatively low concentrations. (b) Irregular

been dated to 36.5–29.8 ^{14}C ka BP in five cores on the Reykjanes Ridge (Lackschewitz and Wallrabe-Adams, 1997). The V2 ash zone exhibits a heterogeneous geochemical signature and coincides with a high input of IRD, sourced from active erosion on the Icelandic ice sheet (Lackschewitz and Wallrabe-Adams, 1997). A number of shards fall within the JM11-19PC 427–439 cm compositional envelope (Fig. 9c), although the wide geochemical spread across all elemental oxides prevents a correlation between the two deposits.

Fig. 9d highlights how the wide geochemical range of the FMAZ III deposit in JM11-19PC straddles the compositional fields for ten of the cryptotephra deposits identified in NGRIP during this time period (between $38,048 \pm 721$ a b2k and $38,826 \pm 740$ a b2k) (Bourne et al., 2013). Thus, none of the glass shard populations from the individual depth intervals between 427 and 439 cm can be exclusively correlated to a single ice-core horizon.

3.4. FMAZ IV

3.4.1. Tephrostratigraphy; JM11-19PC 533–548 cm

A visible thick black macrotephra (6 cm) was deposited during the early stages of DO-12 and after H5, according to the high magnetic susceptibility values (Fig. 4). A rapid increase in shard concentration is evident in the 25–80 μm fraction at 542–543 cm, increasing to ~ 2.9 million shards per 0.5 gdw. Thus, 542–543 cm represents the peak in shard concentration and is suggested to equate to the correct stratigraphical placement of the isochron. The initial major influx in the 80–125 μm fraction is 1 cm below this peak. This slight depth offset could be due to different settling velocities through the ocean, or the movement of heavier material through soft sediment (Enache and Cumming, 2006). Shards at 542–543 cm are yellowish-brown in colour, have a vesicular appearance and display a variety of platy morphologies. In general, the shard concentration profile forms a similar upward tail to that of the 298–303 cm deposit, although the decline in concentration is far more gradual in this horizon; forming a tailed, gradational distribution that covers a ~ 40 cm interval. This can be seen visibly in the core and is reflected in the 25–80 μm fraction, which maintains shard concentrations >1 million per 0.5 g (gdw) at the end of the 10 cm high-resolution sampling interval.

3.4.2. Micro-sedimentology

There are two distinct units in this section. The first occurs between 549 and 543.3 cm and is composed of a massive, moderately-sorted coarse silt with a low concentration of tephra shards, ~ 50 μm in diameter ($n = 20$), distributed randomly within the matrix (Fig. 6f). The second unit identified between 543.3 and 540 cm is composed of moderately-sorted, abundant tephra shards dominated by the 25–80 μm size fraction within a coarse silt host sediment. This second unit has a diffuse contact with the underlying sediment and there are occasional horizontally aligned lenses (~ 1.5 mm) of well-sorted tephra grains up to ~ 140 μm in size (Fig. 6h). The visible tephra component has a similar shard size (25–80 μm) throughout the second unit. The tephra is highly concentrated but poorly mixed within the host sediment (Fig. 6g).

3.4.3. Geochemistry and wider correlations: JM11-19PC 542–543 cm

In total, 71 shard analyses form a homogeneous population (Fig. 10), with 1 clear outlier in the 25–80 μm fraction and two clear outliers in the 80–125 μm fraction. Distinctive geochemical characteristics of the main population are SiO_2 concentrations of ~ 49.0 – 51.4 wt%, K_2O concentrations of ~ 0.4 wt% and TiO_2 and MgO concentrations of ~ 2.6 wt% and ~ 5.8 wt% respectively (Fig. 10). These geochemistries are characteristic of the tholeiitic rock suite, and the latter two oxides suggest a strong affinity to the Grímsvötn system in the Eastern Volcanic Zone of Iceland (Jakobsson et al., 2008) (Fig. 5).

A comparison of the glass shard analyses with deposits from four other marine cores in the Faroes region suggests a strong statistical similarity (SC = 0.98) with the recently discovered 'FMAZ IV' tephra (Wastegård and Rasmussen, 2014). This can be clearly observed on $\text{FeO}_{\text{tot}}/\text{MgO}$ vs TiO_2 and CaO vs MgO biplots (Fig. 10a). JM11-19PC exhibits a tighter distribution of geochemistries in comparison to other cores analysed in the Faroes region, and only glass shards isolated in LINK 15 have a sub-population with a Katla affinity.

Wastegård and Rasmussen (2014) suggest that a potential correlation exists between the FMAZ IV and the V5 ash zone found in two cores on the Reykjanes Ridge, with an age estimate of 46.2–52.5 ^{14}C ka BP (Lackschewitz and Wallrabe-Adams, 1997). The deposit has no coeval IRD signal, but exhibits a heterogeneous geochemical distribution (Lackschewitz and Wallrabe-Adams, 1997). One of the populations from the V5 ash zone in core SO82-7-KAL includes a number of shards which fall within the JM11-19PC 542–543 cm compositional envelope (Fig. 10b). A statistical similarity coefficient of 0.95 suggests a correlation may exist between the two deposits, although the absence of shard concentration profiles prevents a full correlation as the stratigraphic position of the isochron within the Reykjanes Ridge record is uncertain.

A number of basaltic horizons deposited during MIS 3 have also been reported in core PS-2644 in the Iceland Sea, NW of Iceland (Voelker et al., 2000). Two horizons lie in a similar stratigraphic position to JM11-19PC 542–543 cm, based upon the planktonic foraminifera $\delta^{18}\text{O}$ record (Voelker et al., 2000; Wastegård and Rasmussen, 2014). The horizon at 5.18 m within PS-2644 has a relatively homogenous population but exhibits higher TiO_2 , FeO_{tot} and K_2O concentrations than JM11-19PC 542–543 cm. The horizon at 5.22 m is heterogeneous with multiple geochemical populations, although some shards display affinity to the JM11-19PC 542–543 cm compositional envelope (Fig. 10b). The heterogeneity of this deposit, however, makes it difficult to provide a correlative link between the Faroes region and the Iceland Sea.

4. Discussion

4.1. Determining transport and depositional processes

4.1.1. FMAZ II

A striking feature of the FMAZ II deposit is the strong geochemical homogeneity reflected in the JM11-19PC data-set.

horizontally and vertically aligned tephra lenses, composed of abundant, well-sorted glass shards. (c) Isochron position of JM11-19PC at 304–305 cm with a sharp contact of abundant well-sorted tephra. (d) Unit 2 (304.5–298.0 cm) of the FMAZ II deposit; the glass shards are less densely concentrated in the upper part of this unit and more mixed within the host sediment. (ii) FMAZ III deposit (e) Indicative microfacies features with structureless/massive, relatively poorly-sorted matrix of coarse clays and coarse silts, with glass shards distributed in lenses randomly throughout. A high number of mineral grains are also present. (iii) FMAZ IV deposit (f) Moderately-sorted coarse silts with glass shards distributed randomly in low concentrations throughout unit 1 (549.0–543.3 cm) (g) Unit 2 (543.3–540 cm) of the FMAZ IV composed of moderately-sorted, abundant glass shards within a coarse silt host sediment. (h) Isochron position of JM11-19PC 542–543 cm with occasional horizontally aligned lenses of well-sorted and concentrated glass shards (highlighted). The contact between unit 1 and unit 2 is diffuse. (For interpretation of the references to colour in this figure legend, the reader is referred to the web version of this article.)

Glass shard analyses from other cores in the Faroes region reveal a wider scatter (Fig. 7) which has been suggested to represent different phases of the same eruption, although an eruption closely separated in time cannot be excluded (Wastegård et al., 2006). Alternatively, this scatter may result from the operation of bottom currents and the transportation of material from older eruptions to these sites. Glass shards analysed from the JM11-19PC and LINK17 cores exhibit the tightest geochemical populations and plot consistently within the NGRIP 1848.0 m (FMAZ II) compositional envelope. This suggests that deposition was likely controlled by one dominant primary process in the Faroes region and several lines of evidence suggest that this tephra was deposited isochronously, most likely via sea-ice rafting. Firstly, the concentration of coarse-grained shards ($>125\ \mu\text{m}$) is very low in this deposit and the dominant grain size (i.e. 25–80 μm) is typical for primary-airfall or sea-ice rafted deposits. Secondly, the absence of a strong coeval IRD signal suggests that iceberg rafting was not responsible for deposition (Fig. 8). Thirdly, micro-sedimentological features within JM11-19PC suggest the operation of sediment loading. A sudden influx of high tephra concentrations is identified by the sharp contact between units one and two, and the discrete tephra lenses in unit one suggest that glass shards have loaded into the sediment (Fig. 6b). This may result from the rapid influx of tephra to the sediment/water interface at the seabed and the vertical movement of denser tephra shards into the less dense underlying sediment. Thus, the discrete packages of tephra beneath the isochron are interpreted to be the result of gravitational loading. This feature is also apparent in the low shard concentrations beneath the main distribution peak at 304–305 cm (Fig. 4). We postulate that this may be evidence for sea-ice deposition, as we suggest tephra is likely to have fallen to the ocean floor rapidly, following the high accumulation of primary airfall deposits onto seasonal sea-ice. High concentrations of visible tephra occur ~ 2 cm above the load structure at 302–303 cm and although the sedimentary matrix is structureless, this suggests the density contrast was no longer sufficient for the sediment to become unstable and deform. This could represent the diminishing input of tephra into the succession. Importantly, the isochron is placed at 304–305 cm in the JM11-19PC core, marking the sharp contact between the two sedimentary units and the loading of high tephra delivery into the sequence, which is further re-enforced by a peak in shard concentration at this depth interval.

The correlation of this horizon to the SO82-5-V1x-KAL horizon on the Reykjanes Ridge provides further evidence for the operation of sea-ice rafting. The high number of coarse-grained shards (up to 500 μm in diameter) within the V1x horizon suggests that primary airfall is unlikely. Although Lackschewitz and Wallrabe-Adams (1997) propose that the horizon is a product of local sediment gravity flows, the evidence presented here cannot rule out the possibility of sea-ice rafting which was particularly prevalent during the stadial conditions at the time of tephra deposition.

4.1.2. FMAZ IV

The geochemical homogeneity of the FMAZ IV deposit in JM11-19PC and other cores in the Faroes region strongly implies primary deposition. Several lines of evidence suggest that this tephra was deposited isochronously, most likely via primary airfall. Firstly, the concentration of coarse-grained shards ($>80\ \mu\text{m}$) is very low and the dominant grain size (i.e. $<80\ \mu\text{m}$) is typical for atmospherically-derived deposits. Secondly, geochemical similarities between this deposit and the V5 ash zone in core SO82-5, which exhibits no coeval IRD signal, suggests iceberg rafting was not responsible for its deposition. Thirdly, unlike the FMAZ II, the absence of load structures in the microfacies of this deposit suggests a sea-ice component did not assist in tephra delivery to the site. In

addition, a distinct feature of this tephra deposit is an upward tail on the shard concentration profile (Fig. 4). This evidence may suggest greater rates of bioturbation during this period and upward mixing (e.g. Jumars and Wheatcroft, 1989; Abbott et al., 2013; Todd et al., 2014) or re-working by stronger bottom currents during interstadial conditions following primary deposition onto the seafloor. There is also a possibility that material from this one eruption may have been repeatedly overlain at the site following deposition in other regions. Implicit in this interpretation is that movement of particles through the ocean was not as aggregated or as rapid as when it was deposited from the melting of sea-ice and was of insufficient concentration to cause gravitational loading. We believe that these processes are unlikely to have affected the depth and value of the isochron.

The presence of glass shards of Katla composition in the nearby LINK 15 implies that the processes controlling deposition at this particular site were different to those operating at other core locations. Given the absence of loading at JM11-19PC, there is unlikely to be a sea-ice component and thus, the heterogeneity within the LINK 15 deposit may be a reflection of different bottom current transport pathways. Importantly, the isochron is placed at 542–543 cm in the JM11-19PC core, marking the peak in shard concentration and the initial presence of tephra lenses identified within the microfacies. The isochron position also falls within high magnetic susceptibility values in the JM11-19PC core, suggested to equate to the warmth of DO-12, providing further evidence that a sea-ice component is unlikely to have assisted in the deposition of this tephra deposit.

4.1.3. FMAZ III

The diffuse nature of the FMAZ III deposit, which contains multiple peaks in shard concentration, combined with geochemical heterogeneity, suggests either the operation of iceberg rafting and/or post-depositional processes. Iceberg rafting is unlikely due to the absence of a coeval IRD signal (Fig. 8) and low concentrations of coarse-grained shards ($>125\ \mu\text{m}$) (Fig. 4). Instead, the evidence suggests that primary airfall is the dominant transport process, but implies that another process may have operated to modify this depositional signal.

The diagnostic tailed shard distribution and homogeneous geochemistry exhibited by the FMAZ IV has been interpreted to be a signature of bottom current remobilisation and/or bioturbation of material from a single eruption, which implies that these processes alone were insufficient to produce the heterogeneous composition of the FMAZ III deposit. However, the geochemical similarities between this deposit and ten separate volcanic events identified in NGRIP over this time period (Bourne et al., 2013) suggests that the FMAZ III is a tephra zone made up of an amalgamation of glass shards sourced from several closely-timed Grímsvötn eruptions. The sedimentary accumulation rate in the marine environment is most likely insufficient to isolate and stratigraphically separate glass shards from each closely-timed individual eruption as preserved in the ice-core record (Bourne et al., 2013). We postulate that bottom currents and bioturbation further contributed to form the amalgamation of this tephra deposit, following deposition via primary airfall. This is further supported by the microfacies of JM11-19PC, which consists of a structureless mass of sediment with sporadic tephra packages dispersed randomly throughout the sequence, reflecting frequent input into the system and/or remobilisation of shards (Fig. 6). In this instance, the microfacies analysis for FMAZ III cannot help to assign the position of the isochron. Furthermore, this deposit demonstrates that the integrity of the isochron, despite being a product of primary airfall, is compromised by the frequency of eruptions during this period of deposition.

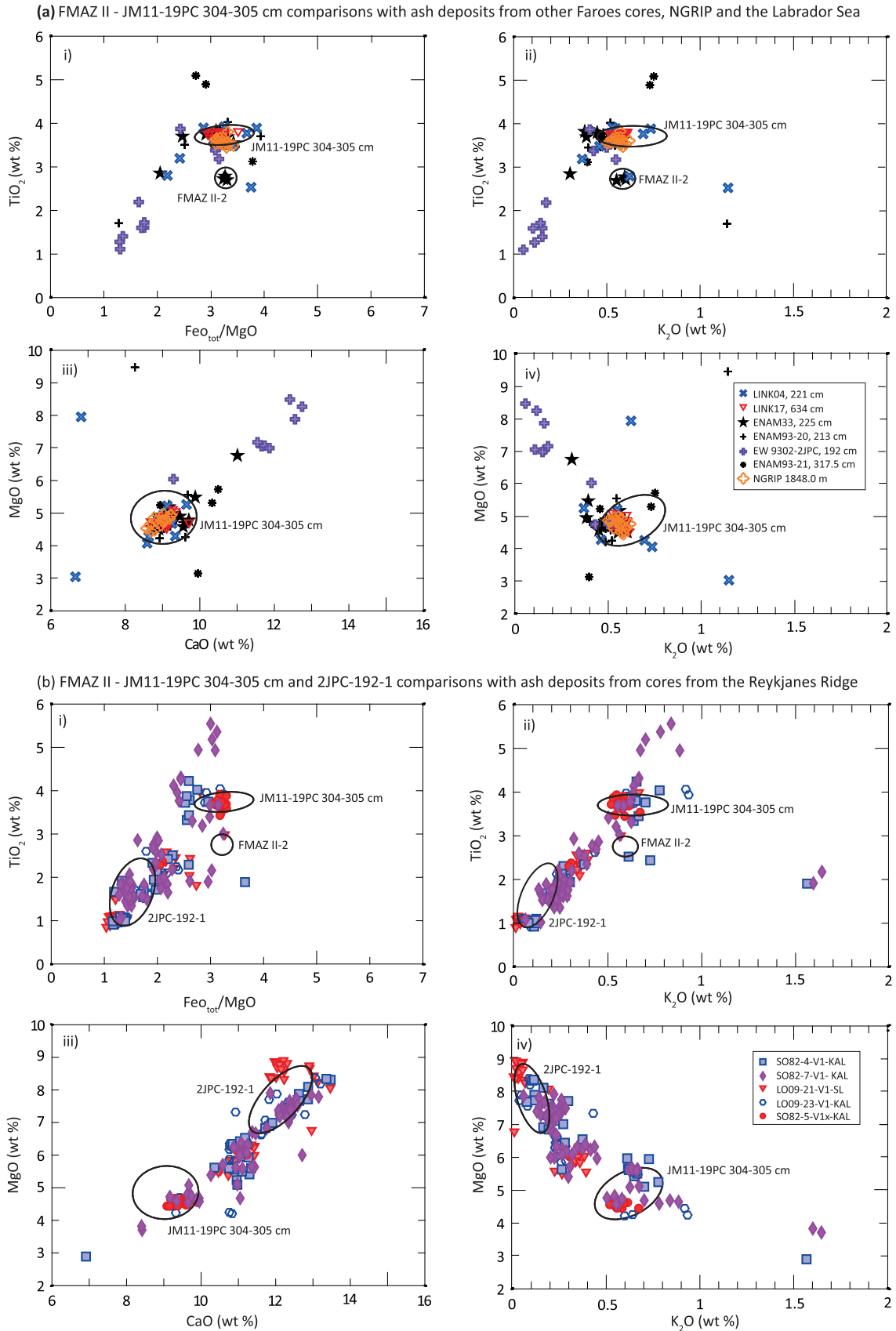


Fig. 7. Major oxide results (wt %) for glass shards from the FMAZ II deposit. (a) (i–iv) The JM11-19PC 304–305 cm compositional envelope is derived from shard analyses obtained from all grain size fractions investigated in this study. An envelope rather than the individual data points are shown for clarity. Geochemical results for other reported FMAZ II deposits in the North Atlantic are shown for comparison and the FMAZ II-2 compositional envelope is defined by [Wastegård et al. \(2006\)](#). Glass shard analyses from six marine cores from the Faroes region and EW9302-2JPC in the Labrador Sea are from [Wastegård et al. \(2006\)](#). Data for NGRIP 1848.0 m from [Davies et al. \(2008\)](#). (b) (i–iv) Geochemical envelopes for the 2JPC-192-1 (a geochemical population present in EW9302-2JPC) and JM11-19PC 304–305 cm deposits compared to V1 and V1-x glass shard analyses derived from five marine cores on the Reykjanes Ridge ([Lackschewitz and Wallrabe-Adams, 1997](#)). Data have all been normalised to 100% total oxide concentrations. Outliers from JM11-19PC have been omitted.

The FMAZ III forms a diachronous surface and whilst the deposit can be useful for marine correlations, its use as a high-precision isochronous tie-point is limited. High sedimentation areas may well preserve well-defined shard concentration peaks with distinct geochemical populations. We refer to this deposit as an ‘ash zone’ and suggest that this term be used solely as a descriptive term to depict the presence of tephra within a core, without any preconceived notions of geochemical characteristics and depositional processes. If horizons can be resolved within the ash zone using techniques outlined above, then the deposit could well reveal discrete isochrons. Implicit in this definition is that the FMAZ II and FMAZ IV are ash zones that form well-defined isochronous horizons.

4.2. The development of a protocol for assessing tephra deposition in the marine environment

Using existing knowledge from previous marine tephra investigations (e.g. Hafliðason et al., 2000; Rasmussen et al., 2003; Wastegård et al., 2006; Brendryen et al., 2010; Abbott et al., 2011, 2013) and the diagnostic signatures of the FMAZs outlined here, we are able to recommend a stepped analytical protocol for resolving tephra depositional pathways in the marine realm (Fig. 11). This procedure highlights the importance of employing contiguous shard concentration profiles, geochemical characteristics and IRD indicators. Micromorphological analysis provides important additional sedimentological evidence for the dominant processes of tephra delivery to the sea floor and supports the correct stratigraphical placement of the isochron. The occurrence of

sedimentary loading has been suggested here to potentially reflect the delivery of tephra to the site via sea-ice. However, distinguishing between sea-ice rafting and primary-airfall is not essential, as sea-ice transportation is unlikely to have affected the position or integrity of the tephra horizon for use as an isochronous marker. Identification of tephra deposits transported by iceberg rafting, however, is crucial.

This protocol also encourages an understanding of ocean currents and the climatic regime associated with tephra deposition. The tephrostratigraphic record from the Faroe-Shetland Channel provides some of the highest concentrations of tephra presently found in the North Atlantic (Wastegård and Rasmussen, 2014). This may be due to its proximity to Iceland and/or due to elevated bottom current transport pathways concentrating material following eruptions. Thus, it is essential to assess whether deposition occurred during stadial or interstadial climates, which exert a control on the strength of bottom currents and subsequently the ability to remobilise previously deposited material. This protocol highlights the importance of using a range of indicators in order to unravel the operation of different depositional mechanisms. We also stress that this protocol is not exhaustive and envisage further iterations and additions based on further work at a network of sites in the North Atlantic to refine the complex interplay of processes that are spatially dependant. Nonetheless, we believe that the protocol outlined in Fig. 11 provides a robust framework and a suite of indicators that will aid in the assessment of depositional processes influencing both tephra and cryptotephra deposits in the marine environment.

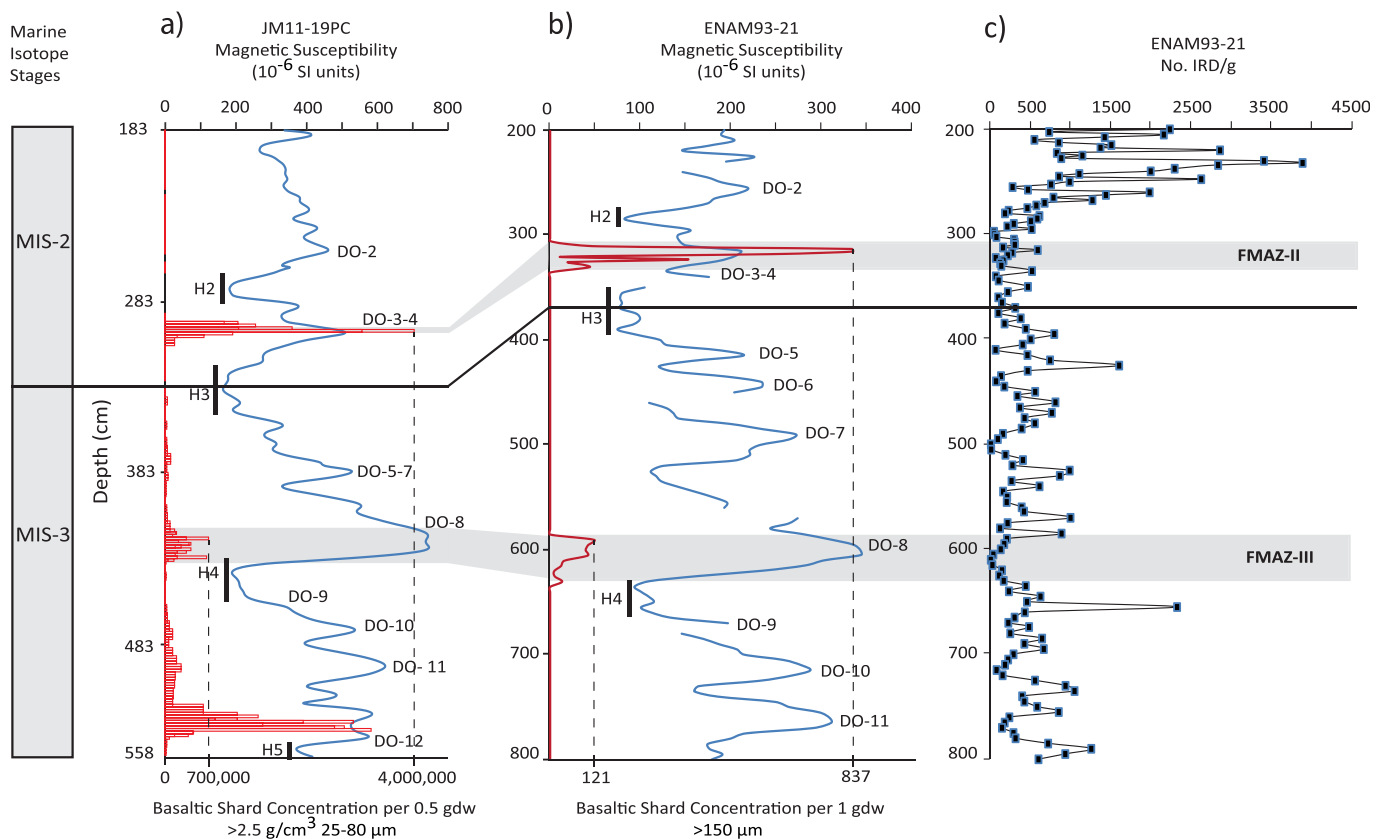
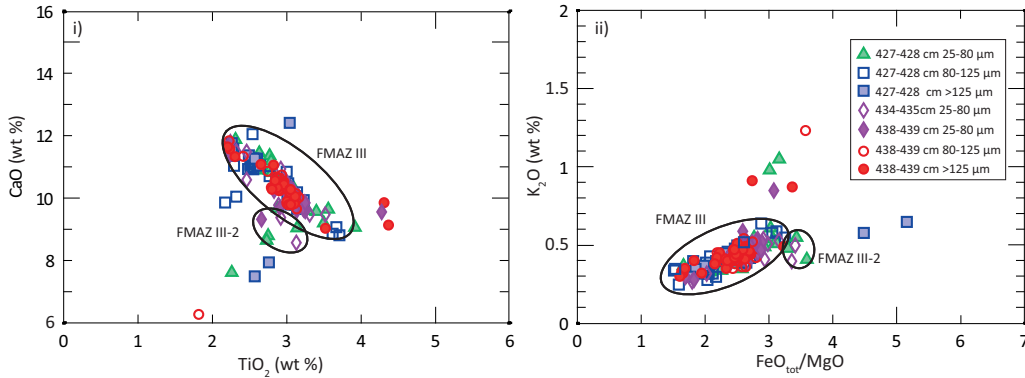
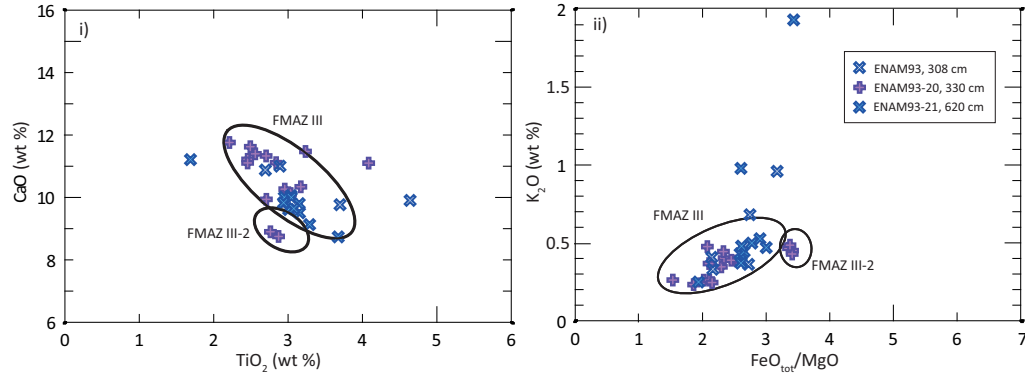


Fig. 8. Comparison of JM11-19PC and ENAM93-21 magnetic susceptibility and tephrostratigraphies to ascertain a corresponding IRD signal. a) Magnetic susceptibility for JM11-19PC with corresponding tephra counts with a density $>2.5 \text{ g/cm}^3$ within the $25\text{--}80 \mu\text{m}$ fraction (gdw = grams dry weight sediment) b) Magnetic susceptibility for ENAM93-21 (Rasmussen et al., 1996) with corresponding tephra counts from the $>150 \mu\text{m}$ fraction (Rasmussen et al., 2003). c) Number of ice-rafted grains $>500 \mu\text{m}$ per gdw (IRD) in ENAM93-21 (Rasmussen et al., 1996). The grey bars represent correlation between records based upon the position of the FMAZ II and FMAZ III horizons in both sequences. H = Heinrich event approximate positions. DO = Dansgaard-Oeschger event following the recommendations in Rasmussen et al. (2014).

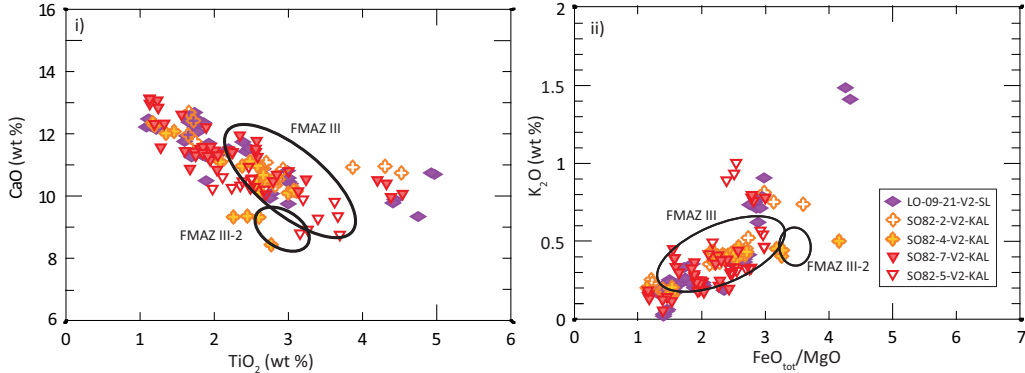
(a) JM11-19PC geochemical distribution of all grain size fractions between 427-439 cm



(b) Comparison of the geochemical populations from JM11-19PC 427-439 cm with ash deposits from marine cores from the Faroes region



(c) Comparison of the geochemical populations from JM11-19PC 427-439 cm with ash deposits from marine cores from the Reykjanes Ridge



(d) Comparison of all grains sizes from JM11-19PC 427-439 cm with 10 horizons from NGRIP

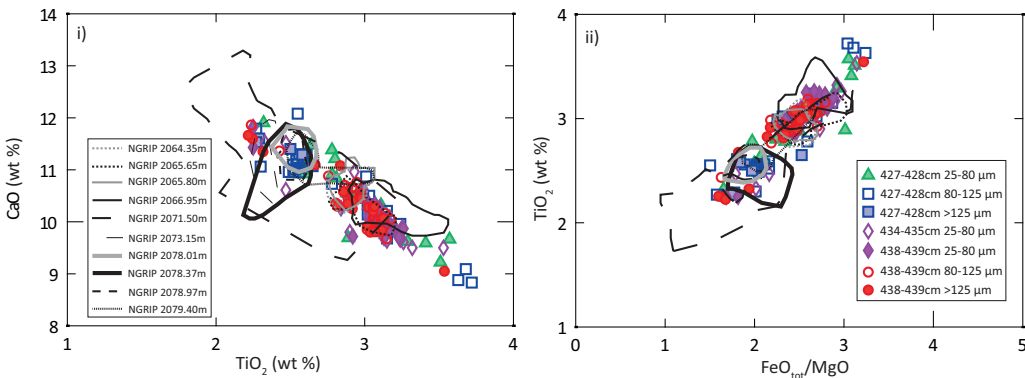
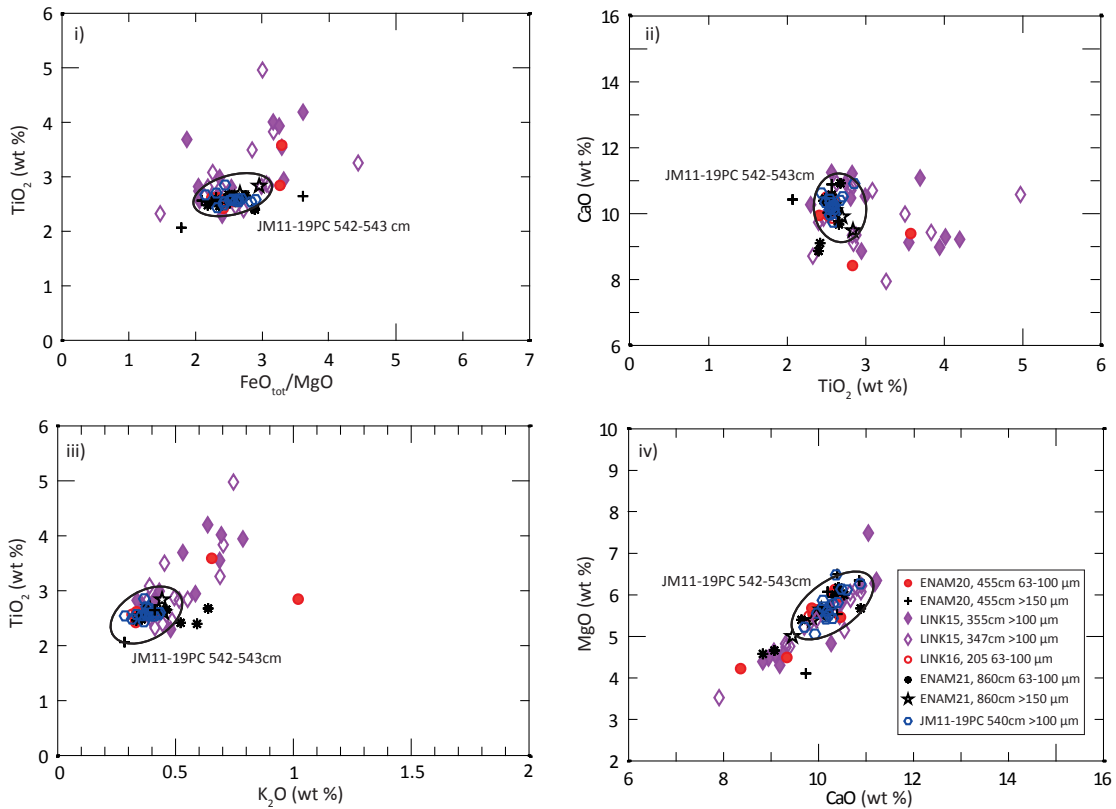


Fig. 9. Major oxide results (wt %) for the FMAZ III deposit identified in JM11-19PC. (a) (i & ii) The FMAZ III compositional envelope is derived from the main geochemical population from 427 to 439 cm in JM11-19PC and the FMAZ III-2 envelope is a sub-population defined by [Wastegård et al. \(2006\)](#). (b) (i & ii) JM11-19PC FMAZ III and FMAZ III-2 envelopes compared to glass shard analyses from three marine cores in the Faroes region ([Wastegård et al., 2006](#)). (c) (i & ii) JM11-19PC FMAZ III and FMAZ III-2 envelopes compared to the V2 ash zone identified in four marine cores on the Reykjanes Ridge ([Lackschewitz and Wallrabe-Adams, 1997](#)). (d) (i & ii) Glass shard analyses from JM11-19PC 427–439 cm compared to ten geochemical compositional envelopes for cryptotephra deposits identified in NGRIP between $38,048 \pm 721$ a b2k and $38,826 \pm 740$ a b2k ([Bourne et al., 2013](#)). The data have all been normalised to 100% total oxide concentrations.

(a) JM11-19PC 542-543 cm comparison with ash deposits from other marine cores in the Faroes region



(b) JM11-19PC 542-543 cm comparison with ash deposits from other marine cores in the Reykjanes Ridges and Iceland Sea

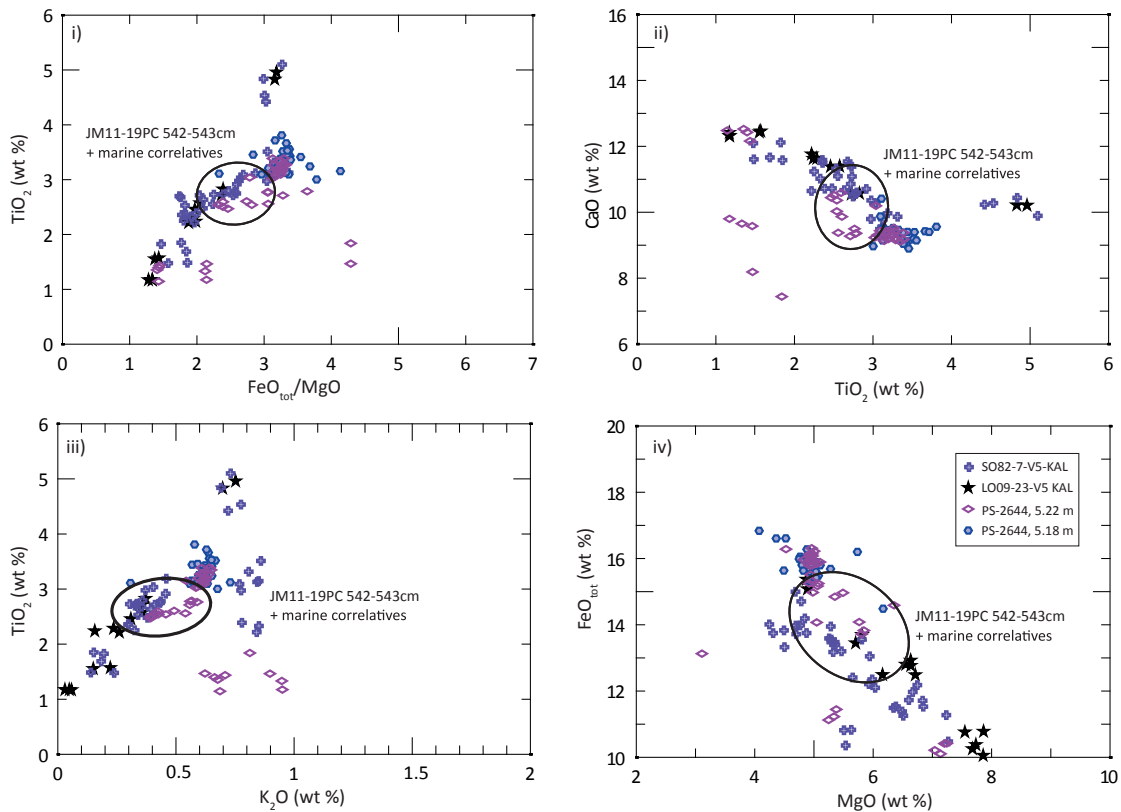


Fig. 10. Major oxide biplots (wt %) for the FMAZ IV deposit in JM11-19PC. a) JM11-19PC 542–543 cm compositional envelope derived from glass shard analyses extracted from all grain-size fractions. (a) (i–iv) This envelope is compared to tephra deposits from four other marine cores from the Faroes region and additional JM11-19PC glass shard analyses reported by [Wastegård and Rasmussen \(2014\)](#). b) Glass shard analyses from JM11-19PC and ENAM93-21 are combined to create a separate compositional envelope named 'JM11-19PC 542–543 cm + marine correlatives'. (b) (i–iv) This envelope is plotted alongside glass shard analyses from the V5 ash zone compiled from two marine cores on the Reykjanes Ridge ([Lackschewitz and Wallrabe-Adams, 1997](#)) and two horizons derived from one marine core in the Iceland Sea ([Voelker et al., 2000](#)). Data have all been normalised to 100% total oxide concentrations. Outliers from JM11-19PC have been omitted.

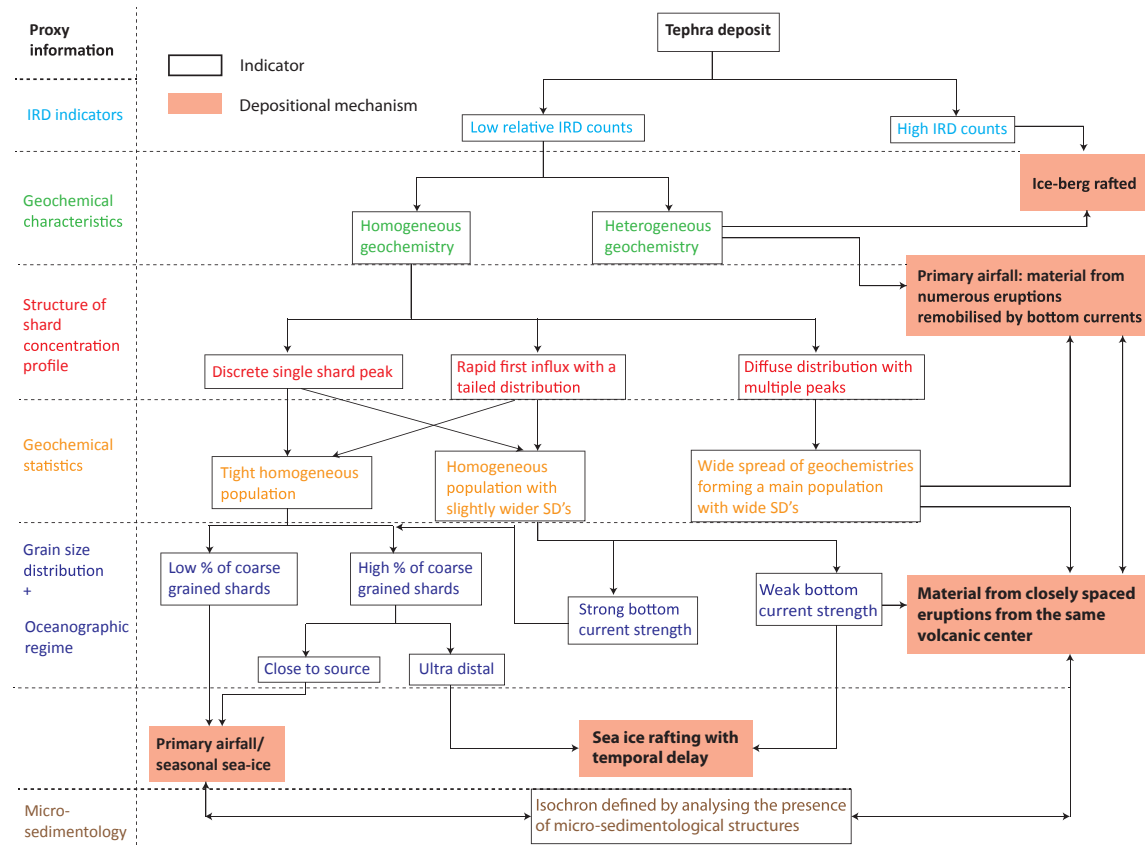


Fig. 11. Protocol for the investigation of primary and secondary depositional processes in marine tephrochronological studies. SD = Standard Deviation.

5. Conclusions

The tephrostratigraphy of a North Atlantic marine core from the southeastern Norwegian Sea has been presented, focussing on three basaltic tephra horizons, referred to as the Faroe Marine Ash Zones. High-resolution contiguous shard concentration profiles, rigorous geochemical characterisation of three separate grain-size fractions and micromorphological techniques are employed to successfully decouple secondary depositional signals. Correlation to previously obtained geochemical data from marine and ice-core archives indicate that i.) the FMAZ III cannot be used as a marine-ice isochron in high-precision studies, unless individual homogeneous horizons can be resolved in cores from high sedimentation areas, and ii.) the FMAZ II and IV are well-resolved primary deposits that can be used as isochrons for high-precision correlation studies. Key primary features of these two horizons are a well-defined shard concentration peak, homogeneous geochemical signatures, a high percentage of fine-grained shards and an absence of a coeval IRD signal. The diagnostic features of each of the three tephra deposits have enabled the development of a protocol to assess depositional pathways for future marine tephrochronological studies in the North Atlantic. This protocol highlights the need for adopting a rigorous stratigraphic investigation with intensive geochemical acquisition. When these techniques are combined with an understanding of site specific palaeoceanographic processes, this enables the decoupling of the complex interplay of processes that operated in the North Atlantic during the last glacial period. Where sufficient material exists, we recommend the use of micromorphology to provide further discriminatory evidence for the dominant method of tephra delivery to the sea floor. However, as yet, it is uncertain how useful this technique will be for cryptotephra deposits

comprised of low concentrations of glass shards. Moreover, this study reinforces the importance of employing down-core high-resolution shard concentration profiles for resolving transport and depositional mechanisms and we recommend routine use of this technique in tephrochronological studies. The protocol outlined in this study represents an important step towards optimising the application of marine-based tephra and cryptotephra isochrons for correlating to coeval deposits in the Greenland ice-cores and other disparate records.

Acknowledgements

This study forms part of the Tephra constraints on Rapid Climate Events (TRACE) project which aims to correlate tephra found in the Greenland Ice Cores and North Atlantic marine cores in order to understand mechanisms of abrupt climate change during the last glacial period. The research leading to these results has received funding from the European Research Council under the European Union's Seventh Framework Programme (FP7/2007-2013)/ERC grant agreement n° [259253]. AJG, SMD and PMA acknowledge the support of the Climate Change Consortium of Wales (C3W). AJG acknowledges the QRA for the Postgraduate Research Award for thin-section preparation at Royal Holloway, University of London. We thank the captain and crew of the R-V Jan Mayen for their assistance in the retrieval of core JM11-19PC. We are grateful for the assistance of Dr Chris Hayward with the use of the electron microprobe at the Tephrochronology Analytical Unit, University of Edinburgh. We are grateful to Professor Stefan Westergård for providing geochemical data for the FMAZ IV and Dr Hans-Joachim Wallrabe-Adams for providing geochemical data for the V ash zones. Sune Rasmussen, Sean Pyne-O'Donnell and Sabine Wulf are

thanked for their constructive reviews of this manuscript. This paper contributes to the EU-funded COST ACTION INTIMATE (ES0907) (<http://cost-es0907.geoenvi.org/>) and to the INTREPID (Enhancing tephrochronology as a global research tool through improved fingerprinting and correlation techniques and uncertainty modelling) – an INQUA INTAV-led project (International Focus Group on Tephrochronology and Volcanism, project no. 0907).

Appendix A. Supplementary data

Supplementary data related to this article can be found at <http://dx.doi.org/10.1016/j.quascirev.2014.04.031>.

References

- Abbott, P.M., Davies, S.M., 2012. Volcanism and the Greenland ice-cores: the tephra record. *Earth Sci. Rev.* 115, 173–191.
- Abbott, P.M., Davies, S.M., Austin, W.E.N., Pearce, N.J.G., Hibbert, F.D., 2011. Identification of cryptotephra horizons in a North East Atlantic marine record spanning marine isotope stages 4 and 5a (~60,000–82,000 a b2k). *Quat. Int.* 246, 177–189.
- Abbott, P.M., Austin, W.E.N., Davies, S.M., Pearce, N.J.G., Hibbert, F.D., 2013. Cryptotephrochronology of the Eemian and the Last Interglacial-glacial transition in the North East Atlantic. *J. Quat. Sci.* 28, 501–524.
- Abbott, P.M., Austin, W.E.N., Davies, S.M., Pearce, N.J.G., Rasmussen, T.L., Wastegård, S., Brendryen, J., 2014. Re-evaluation and extension of the Marine Isotope Stage 5 tephrostratigraphy of the Faroe Islands region: the cryptotephra record. *Palaeogeogr. Palaeoclimatol. Palaeoecol.* (in press).
- Austin, W.E.N., Hibbert, F.D., 2012. Tracing time in the ocean: a brief review of chronological constraints (60–8 kyr) on North Atlantic marine event-based stratigraphies. *Quat. Sci. Rev.* 36, 28–37.
- Austin, W.E.N., Wilson, L.J., Hunt, J.B., 2004. The age and chronostratigraphical significance of North Atlantic Ash Zone II. *J. Quat. Sci.* 19, 137–146.
- Austin, W.E.N., Hibbert, F.D., Rasmussen, S.O., Peters, C., Abbott, P.M., Bryant, C.L., 2012. The synchronization of palaeoclimatic events in the North Atlantic region during Greenland Stadial 3 (ca 27.5 to 23.3 kyr b2k). *Quat. Sci. Rev.* 36, 154–163.
- Begét, J., Mason, O., Anderson, P., 1992. Age, extent and climatic significance of the c. 3400 BP Aniakchak tephra, western Alaska, USA. *Holocene* 2, 51–56.
- Blockley, S.P.E., Lane, C.S., Lotter, A.F., Pollard, A.M., 2007. Evidence for the presence of the Vedde Ash in Central Europe. *Quat. Sci. Rev.* 26, 3030–3036.
- Blockley, S.P.E., Pyne-O'Donnell, S.D.F., Lowe, J.J., Matthews, I.P., Stone, A., Pollard, A.M., Turney, C.S.M., Molyneux, E.G., 2005. A new and less destructive laboratory procedure for the physical separation of distal glass tephra shards from sediments. *Quat. Sci. Rev.* 16–17, 1952–1960.
- Borchardt, G.A., Aruscavage, P.J., Millard Jr., H., 1972. Correlation of the Bishop ash, a Pleistocene marker bed, using instrumental neutron activation analysis. *J. Sediment. Petrol.* 42, 201–206.
- Bourne, A.J., 2012. The Late Quaternary Tephrochronology of the Adriatic Region; Implications for the Synchronization of Marine Records (Unpublished PhD thesis). Royal Holloway, University of London, UK.
- Bourne, A.J., Davies, S.M., Abbott, P.M., Rasmussen, S.O., Steffensen, J.P., Svensson, A., 2013. Revisiting the Faroe Marine Ash Zone III in two Greenland ice Cores: implications for marine-ice-core correlations. *J. Quat. Sci.* 28, 641–646.
- Boyle, J.E., 1994. Tephra in Lake Sediments: an Unambiguous Geochronological Marker? (Ph.D. thesis) University of Edinburgh.
- Bramlette, M.N., Bradley, W.H., 1941. Geology and Biology of North Atlantic Deep-sea Cores Between Newfoundland and Ireland: I. Lithology and Geologic Interpretation. U.S. Geological Survey Professional Paper. 196-A, pp. 1–34.
- Brendryen, J., Hafliðason, H., Sejrup, H.P., 2010. Norwegian Sea tephrostratigraphy of marine isotope stages 4 and 5: prospects and problems for tephrochronology in the North Atlantic region. *Quat. Sci. Rev.* 29, 847–864.
- Davies, S.M., Wastegård, S., Rasmussen, T.L., Svensson, A., Johnsen, S.J., Steffensen, J.P., Andersen, K.K., 2008. Identification of the Fugloyarbanki tephra in the NGRIP ice core: a key tie-point for marine and ice-core sequences during the Last Glacial period. *J. Quat. Sci.* 23, 409–414.
- Davies, S.M., Wastegård, S., Abbott, P.M., Barbante, C., Bigler, M., Johnsen, S.J., Rasmussen, T.L., Steffensen, J.P., Svensson, A., 2010. Tracing volcanic events in the NGRIP ice-core and synchronising North Atlantic marine records during the Last Glacial period. *Earth Planet. Sci. Lett.* 294 (1–2), 69–79.
- Davies, S.M., Abbott, P.M., Pearce, N.J.G., Wastegård, S., Blockley, S.P.E., 2012. Integrating the INTIMATE records using tephrochronology: rising to the challenge. *Quat. Sci. Rev.* 36, 11–27.
- Davies, S.M., Abbott, P.M., Meara, R.H., Pearce, N.J.G., Austin, W.E.N., Chapman, M.R., Svensson, A., Bigler, M., Rasmussen, 2014. A North Atlantic tephra framework for 130,000–60,000 years b2k: new tephra discoveries, marine based-correlations and future challenges. *Quat. Sci. Rev.* 106, 101–121.
- Enache, M.D., Cumming, B.F., 2006. The morphological and optical properties of volcanic glass: a tool to assess density-induced vertical migration of tephra in sediment cores. *J. Paleolimnol.* 35, 661–667.
- Froggatt, P.C., Gosson, G.J., 1982. Techniques for the Preparation of Tephra Samples for Mineral or Chemical Analysis and Radiometric Dating, vol. 23. Geology Department, Victoria University of Wellington Publication, pp. 1–12.
- Gehrels, M.J., Lowe, D.J., Hazell, Z.J., Newnham, R.M., 2006. A continuous 5300-yr Holocene cryptotephrostratigraphic record from northern New Zealand and implications for tephrochronology and volcanic hazard assessment. *Holocene* 16, 173–187.
- Hafliðason, H., Eiríksson, J., van Kreveld, S., 2000. The tephrochronology of Iceland and the North Atlantic region during the Middle and Late Quaternary: a review. *J. Quat. Sci.* 15, 3–22.
- Hayward, C., 2012. High spatial resolution electron probe microanalysis of tephra and melt inclusions without beam-induced chemical modification. *Holocene* 22, 119–125.
- Jakobsson, S.P., 1979. Petrology of recent basalts of the Eastern Volcanic Zone, Iceland. *Acta Nat. Isl.* 26, 1–103.
- Jakobsson, S.P., Jónasson, K., Sigurdsson, I.A., 2008. The three igneous rock suites of Iceland. *Jökull* 58, 117–138.
- Jumars, P.A., Wheatcroft, R.A., 1989. Responses of benthos to changing food quality and quantity, with a focus on deposit feeding and bioturbation. In: Berger, W.H., Smetacek, V.S., Wefer, G. (Eds.), *Productivity of the Ocean: Present and Past*. Wiley, New York, pp. 235–253.
- Kuhs, M., Austin, W.E.N., Abbott, P.M., Hodell, D.A., 2014. Iceberg-rafted tephra as a potential tool for the reconstruction of ice-sheet processes and ocean surface circulation in the glacial North Atlantic. In: Austin, W.E.N., Abbott, P.M., Davies, S.M., Pearce, N.J.G., Wastegård, S. (Eds.), *Marine Tephrochronology*, Geological Society of London Special Publication, vol. 398.
- Lackschewitz, K.S., Wallrabe-Adams, H.J., 1997. Composition and origin of volcanic ash zones in Late Quaternary sediments from the Reykjanes Ridge: evidence for ash fallout and ice rafting. *Mar. Geol.* 136, 209–224.
- Lane, C.S., Andric, M., Cullen, V.L., Blockley, S.P.E., 2011. The occurrence of distal Icelandic and Italian tephra in the Lateglacial of Lake Bled, Slovenia. *Quat. Sci. Rev.* 30, 1013–1018.
- Larsen, G., 1981. Tephrochronology by microprobe glass analysis. In: Self, S., Sparks, R.S.J. (Eds.), *Tephra Studies as a Tool in Quaternary Research*, pp. 95–102.
- Larsen, G., Eiríksson, J., Knudsen, K.L., Heinemeier, J., 2002. Correlation of late Holocene terrestrial and marine tephra markers, north Iceland: implications for reservoir age changes. *Polar Res.* 21, 283–290.
- Lowe, D.J., 2011. Tephrochronology and its application: a review. *Quat. Geochronol.* 6, 107–153.
- Lowe, J.J., Rasmussen, S.O., Björck, S., Hoek, W.Z., Steffensen, J.P., Walker, M.J.C., Yu, Z.C., 2008. Synchronisation of palaeoenvironmental events in the North Atlantic region during the last termination: a revised protocol recommended by the INTIMATE group. *Quat. Sci. Rev.* 27, 6–17.
- Mackie, E., Davies, S.M., Turney, C.S.M., Dobbey, K., Lowe, J.J., 2002. The use of magnetic separation techniques to detect basaltic microtephra in glacial-interglacial transition (LGIT; 15–10 ka cal. BP) sediment sequences in Scotland. *Scott. J. Geol.* 38, 21–30.
- Manville, V., Wilson, C.J.N., 2004. Vertical density currents: a review of their potential role in the deposition and interpretation of deep-sea ash layers. *J. Geol. Soc.* 161, 947–958.
- Matthews, I.P., Palmer, A.P., Folkes, H., Trincardi, F., 2011. Understanding tephra layers in marine sediments, the potential of thin section micromorphology to investigate depositional and taphonomic processes. In: *Marine Tephrochronology Meeting*. Geological Society London, UK, 26 October, 2011.
- van der Meer, J.M., Menzies, J., 2011. The micromorphology of unconsolidated sediments. *Sediment. Geol.* 238, 213–232.
- Michels, K.H., 2000. Inferring maximum geostrophic current velocities in the Norwegian-Greenland Sea from settling velocity measurements of sediment surface samples: methods, application, and results. *J. Sediment. Res.* 70, 1036–1050.
- Óladóttir, B.A., Sigmarsson, O., Larsen, G., Thordarson, T., 2008. Katla volcano, Iceland: magma composition, dynamics and eruption frequency as recorded by Holocene tephra layers. *Bull. Volcanol.* 70, 475–493.
- Palmer, A.P., Lee, J.A., Kemp, R.A., Carr, S.J., 2008. Revised Laboratory Procedures for the Preparation of Thin Sections from Unconsolidated Material. Unpublished Internal Report. Royal Holloway, University of London.
- Pearce, N.J.G., Abbott, P.M., Martin-Jones, C., 2014. Microbeam methods for the analysis of glass in fine-grained tephra deposits: a SMART perspective on current and future trends. In: Austin, W.E.N., Abbott, P.M., Davies, S.M., Pearce, N.J.G., Wastegård, S. (Eds.), *Marine Tephrochronology*, Geological Society of London Special Publication, vol. 398.
- Pyne-O'Donnell, S.D.F., Hughes, P.D.M., Froese, D.G., Jensen, B.J.L., Kuehn, S.C., Mallon, G., Amesbury, M.J., Charman, D.J., Daley, T.J., Loader, N.J., Mauquoy, D., Street-Perrott, F.A., Woodman-Ralph, J., 2012. High-precision ultra-distal Holocene tephrochronology in North America. *Quat. Sci. Rev.* 52, 6–11.
- Rasmussen, S.O., Bigler, M., Blockley, S.P.E., Blunier, T., Borchardt, S.L., Clausen, H.B., Cvijanovic, I., Dahl-Jensen, D., Johnsen, S.J., Fischer, H., Gkinis, V., Guillevic, M., Hoek, W.Z., Lowe, J.J., Pedro, J., Popp, T., Seierstad, I., Steffensen, J.P., Svensson, A.M., Vallelonga, P., Vinther, B.M., Walker, M.J.C., Wheatley, J.J., Winstrop, M., 2014. A framework for robust naming and correlation of past abrupt climatic changes during the recent glacial period based on three synchronised Greenland ice-cores. *Quat. Sci. Rev.* 106, 14–28.
- Rasmussen, T.L., Thomsen, E., Tjeerd, C.E., Weering, V., Labeyrie, L., 1996. Rapid changes in surface and deep water conditions at the Faroe Margin during the last 58,000 years. *Palaeoceanography* 11, 757–771.

- Rasmussen, T.L., Wastegård, S., Kuijpers, A., van Weering, T.C.E., Heinemeier, J., Thomsen, E., 2003. Stratigraphy and distribution of tephra layers in marine sediment cores from the Faeroe Islands, North Atlantic. *Mar. Geol.* 199, 263–277.
- Ruddiman, W.F., Glover, L.K., 1972. Vertical mixing of ice rafted volcanic ash in north Atlantic sediments. *Geol. Soc. Am. Bull.* 83, 2817–2836.
- Sparks, R., 1981. Triggering of volcanic eruptions by earth tides. *Nature* 290, 448.
- Stärz, M., Gong, X., Stein, R., Darby, D.A., Kauker, F., Lohmann, G., 2012. Glacial shortcut of Arctic sea-ice transport. *Earth Planet. Sci. Lett.* 257–358, 257–267.
- Svensson, A., Andersen, K.K., Bigler, M., Clausen, H.B., Dahl-Jensen, D., Davies, S.M., Johnsen, S.J., Muscheler, R., Parrenin, F., Rasmussen, S.O., Röthlisberger, R., Seierstad, I., Steffensen, J.P., Vinther, B.M., 2008. A 60 000 year Greenland stratigraphic ice core chronology. *Clim. Past* 4, 47–57.
- Todd, J.A., Austin, W.E.N., Abbott, P.M., 2014. Quantifying bioturbation of a simulated ash fall event. In: Austin, W.E.N., Abbott, P.M., Davies, S.M., Pearce, N.J.G., Wastegård, S. (Eds.), *Marine Tephrochronology*, Geological Society of London Special Publication, vol. 398.
- Turney, C.S.M., 1998. Extraction of rhyolitic ash from minerogenic lake sediments. *J. Paleolimnol.* 19, 199–206.
- Voelker, A.H.L., Grootes, P.M., Nadeau, M.J., Sarnthein, M., 2000. Radiocarbon levels in the Iceland Sea from 25–53 kyr and their link to the Earth's magnetic field intensity. *Radiocarbon* 42, 437–452.
- Walden, J., Oldfield, F., Smith, J., 1999. *Environmental Magnetism: a Practical Guide*. Quaternary Research Association. Technical Guide No. 6.
- Wallrabe-Adams, H.J., Lackschewitz, K.S., 2003. Chemical composition, distribution, and origin of silicic volcanic ash layers in the Greenland-Iceland-Norwegian Sea: explosive volcanism from 10 to 300 ka as recorded in deep sea sediments. *Mar. Geol.* 19, 273–293.
- Wastegård, S., Rasmussen, T.L., Kuijpers, A., Nielsen, T., van Weering, T.C.E., 2006. Composition and origin of ash zones from Marine Isotope Stages 3 and 2 in the North Atlantic. *Quat. Sci. Rev.* 25, 2409–2419.
- Wastegård, S., Rasmussen, T.L., 2014. Faroe Marine Ash Zone IV – a new MIS3 ash zone of the Faroe Islands margin. In: Austin, W.E.N., Abbott, P.M., Davies, S.M., Pearce, N.J.G., Wastegård, S. (Eds.), *Marine Tephrochronology*, Geological Society of London Special Publication, vol. 398.
- Wiesner, M.G., Wang, Y., Zheng, L., 1995. Fallout of volcanic ash to the deep South China Sea induced by the 1991 eruption of Mount Pinatubo (Philippines). *Geology* 23, 885–888.